Neurobiology of Disease

A Farnesyltransferase Inhibitor Restores Cognitive Deficits in *Tsc2*$^{+/-}$ Mice through Inhibition of Rheb1

Hiroko Sugiura,[1*] Tadayuki Shimada,[1*] Keiko Moriya-Ito,[1] Jun-Ichi Goto,[3] Hiroki Fujiwara,[3] Rie Ishii,[2] Hiroshi Shitara,[2] Choji Taya,[2] Satoshi Fujii,[3] Toshiyuki Kobayashi,[4] Okio Hino,[4] Paul F. Worley,[5] and Kanato Yamagata[1,6]

[1]Laboratory of Synaptic Plasticity, Tokyo Metropolitan Institute of Medical Science, Tokyo 156-8506, Japan, [2]Laboratory for Transgenic Technology, Tokyo Metropolitan Institute of Medical Science, Tokyo 156-8506, Japan, [3]Department of Physiology, Yamagata University School of Medicine, Yamagata 990-9585, Japan, [4]Department of Pathology and Oncology, Juntendo University School of Medicine, Tokyo 113-8421, Japan, [5]Department of Neuroscience, Johns Hopkins University School of Medicine, Baltimore, Maryland 21205, and [6]Department of Psychiatry, Takada Nishishiro Hospital, Niigata 943-0834, Japan

Tuberous sclerosis complex (TSC) is caused by mutations in *Tsc1* or *Tsc2*, whose gene products inhibit the small G-protein Rheb1. Rheb1 activates mTORC1, which may cause refractory epilepsy, intellectual disability, and autism. The mTORC1 inhibitors have been used for TSC patients with intractable epilepsy. However, its effectiveness for cognitive symptoms remains unclear. We found a new signaling pathway for synapse formation through Rheb1 activation, but not mTORC1. Here, we show that treatment with the farnesyltransferase inhibitor lonafarnib increased unfarnesylated (inactive) Rheb1 levels and restored synaptic abnormalities in cultured *Tsc2*$^{+/-}$ neurons, whereas rapamycin did not enhance spine synapse formation. Lonafarnib treatment also restored the plasticity-related Arc (activity-regulated cytoskeleton-associated protein) expression in cultured *Tsc2*$^{+/-}$ neurons. Lonafarnib action was partly dependent on the Rheb1 reduction with syntenin. Oral administration of lonafarnib increased unfarnesylated protein levels without affecting mTORC1 and MAP (mitogen-activated protein (MAP)) kinase signaling, and restored dendritic spine morphology in the hippocampi of male *Tsc2*$^{+/-}$ mice. In addition, lonafarnib treatment ameliorated contextual memory impairments and restored memory-related Arc expression in male *Tsc2*$^{+/-}$ mice *in vivo*. Heterozygous *Rheb1* knockout in male *Tsc2*$^{+/-}$ mice reproduced the results observed with pharmacological treatment. These results suggest that the Rheb1 activation may be responsible for synaptic abnormalities and memory impairments in *Tsc2*$^{+/-}$ mice, and its inhibition by lonafarnib could provide insight into potential treatment options for TSC-associated neuropsychiatric disorders.

Key words: FTI; memory; neural activity; spine morphology; synaptic plasticity; TSC

Significance Statement

Tuberous sclerosis complex (TSC) is an autosomal-dominant disease that causes neuropsychiatric symptoms, including intractable epilepsy, intellectual disability (ID) and autism. No pharmacological treatment for ID has been reported so far. To develop a pharmacological treatment for ID, we investigated the mechanism of TSC and found that Rheb1 activation is responsible for synaptic abnormalities in TSC neurons. To inhibit Rheb1 function, we used the farnesyltransferase inhibitor lonafarnib, because farnesylation of Rheb1 is required for its activation. Lonafarnib treatment increased inactive Rheb1 and recovered proper synapse formation and plasticity-related Arc (activity-regulated cytoskeleton-associated protein) expression in TSC neurons. Furthermore, *in vivo* lonafarnib treatment restored contextual memory and Arc induction in TSC mice. Together, Rheb1 inhibition by lonafarnib could provide insight into potential treatments for TSC-associated ID.

Received Mar. 2, 2021; revised Jan. 14, 2022; accepted Jan. 17, 2022.

Author contributions: K.Y. designed research; H. Sugiura, T.S., K.M.-I., J.-I.G., H.F., R.I., H. Shitara, C.T., S.F., T.K., O.H., P.F.W., and K.Y. performed research; T.S. wrote the paper.

This work was supported in part by Japan Society for the Promotion of Science KAKENHI Grants-in-Aid for Scientific Research JP25293239 and JP18H02536 (to K.Y.); Japan Agency for Medical Research and Development Grant JP18ek0109311/19ek0109311h0002/20ek0109311h0003 (to K.Y.); the SENSHIN Medical Research Foundation; the Japan Epilepsy Research Foundation; and the Tokumori Yasumoto Memorial Trust for Research on Tuberous Sclerosis Complex and Related Rare Neurological Diseases (to K.Y.). We thank Shin Yasuda for technical assistance.

*H.S. and T.S. contributed equally to this work.

The authors declare no competing financial interests.

Correspondence should be addressed to Kanato Yamagata at yamagata-kn@igakuken.or.jp.

https://doi.org/10.1523/JNEUROSCI.0449-21.2022

Introduction

Tuberous sclerosis complex (TSC) is caused by a heterozygous mutation in either the *Tsc1* or *Tsc2* gene, leading to the activation of mTORC1 signaling (Lipton and Sahin, 2014). TSC can involve any tissue or organ, but the CNS is one of the most commonly affected organs; its effects include epilepsy, subependymal giant cell astrocytoma (SEGA), and TSC-associated neuropsychiatric disorders (TANDs). TAND symptoms consist of cognitive, behavioral, and psychiatric disorders, such as intellectual disability, autism, and specific neuropsychological deficits (Curatolo et al., 2008, 2015). The role of the mammalian target of rapamycin

(mTOR) pathway in brain development and function has been intensively studied both *in vitro* and *in vivo*, and mTOR inhibitors [everolimus and sirolimus (rapamycin)] are used to treat SEGA and angiomyolipoma in TSC patients. Thus far, however, everolimus has not been shown to significantly improve neurocognitive functions (memory, attention, executive function, and behavior) in TSC patients (Overwater et al., 2019).

Dendritic spines are the postsynaptic structure of excitatory synapses. The structural plasticity of dendritic spines is tightly correlated with synaptic function and memory. Indeed, a variety of cognitive disorders are accompanied by disease-related changes in dendritic spine morphology (Penzes et al., 2011). In rodent models of TSC, neuronal spine synapse formation was impaired; however, rapamycin did not restore mature spine formation (Yasuda et al., 2014). Thus, mTOR inhibition may not be effective for spine recovery in TSC neurons. This might be related to the reason why rapamycin failed to improve cognitive symptoms in TSC patients.

Tsc1 and Tsc2 form a complex that inhibits the small GTP-binding protein Rheb1, which activates mTORC1 in a GTP-dependent manner (Inoki et al., 2003). We previously showed that the activation of Rheb1, but not of mTORC1, causes synaptic abnormalities via the PDZ protein syntenin1, and that Rheb1 inhibition restored spine synapse formation in $Tsc2^{+/-}$ neurons (Yasuda et al., 2014; Sugiura et al., 2015). Mutation in *Rheb1* gene have been reported to cause intellectual disability in human patients (Reijnders et al., 2017), which is partly consistent with our observations. Thus, TSC–Rheb1 signaling may play an important role in dendritic spine and intellectual development.

The Rheb1 sequence terminates with CSVM, which corresponds to the CAAX box, which is farnesylated (A is an aliphatic amino acid; X is the C-terminal amino acid.). Farnesyltransferase (FTase) preferentially recognizes proteins whose sequences end in serine, methionine, glutamine, or alanine. This modification may localize Rheb1 to lysosomal membranes, followed by its activation (Clark et al., 1997). On the other hand, proteins with the CAAX box whose sequences end in leucine are also modified by geranylgeranyl protein transferase-1 (Casey and Seabra, 1996). K-Ras and N-Ras are not only farnesylated but also geranylgeranylated (Whyte et al., 1997). This geranylgeranylation may provide mutated Ras proteins with resistance to farnesyltransferase inhibitors (FTIs). However, Rheb1 is modified by only farnesylation and does not undergo geranylgeranylation (Clark et al., 1997), indicating that FTIs may efficiently inhibit activation of the Rheb1 protein rather than the Ras protein.

We demonstrated that treatment with FTIs, but not rapamycin, restored spine synapse formation in $Tsc2^{+/-}$ rat neurons (Yasuda et al., 2014). Thus, Rheb1 could be a potential pharmacological target for the treatment of TAND symptoms. A direct inhibitor for Rheb1 was recently developed; however, its IC_{50} is higher than those of FTIs (Mahoney et al., 2018), and the *in vivo* safety has not been characterized yet. Herein, we report the effectiveness of FTIs on cognitive deficits in a mouse model of TSC through the inhibition of Rheb1 and also show that this mechanism may confer a therapeutic advantage.

Materials and Methods

Mice. $Tsc2^{+/-}$ and *Rheb1*-floxed mice were generated previously (Kobayashi et al., 1999; Zou et al., 2011). *CaMKII-Cre;*$Rheb1^{flox/+}$ progeny were generated by crossing *CaMKII-Cre* mice with $Rheb1^{flox/+}$ mice. These progenies were then crossed with $Tsc2^{+/-}$ mice to yield $Tsc2^{+/-}$; *CaMKII-Cre;*$Rheb1^{flox/+}$ mice. Only male animals were used in the behavioral experiments. Mice were of mixed genetic backgrounds (C57BL/6J and 129 Sv). All mice were group housed and maintained under a 12 h light/dark cycle. All animals were treated in accordance with the guidelines of the Animal Care and Use Committee of the Tokyo Metropolitan Institute of Medical Science and the Yamagata University School of Medicine.

Cell culture, transfection, and immunostaining. HEK293 T cells were transfected with FLAG-Rheb1 and/or EGFP-syntenin expression vector. The cells were treated with 2 μM lonafarnib (catalog #S2797, Selleck) and 20 μM MG132 (catalog #M2400, LKT Labs). The primary culture and transfection of mouse hippocampal neurons (P 0–1) have been previously described (Yasuda et al., 2014; Sugiura et al., 2015). Cultured neurons were maintained in Neurobasal Medium (catalog #21103–049, Thermo Fisher Scientific) supplemented with B-27 supplement (catalog #17504–044, Thermo Fisher Scientific) and Antibiotic-Antimycotic (catalog #15240–062, Thermo Fisher Scientific). Neurons at 7 d in *vitro* (DIV7) were transfected with EGFP expression vector using Lipofectamine 2000 (catalog #11668–019, Thermo Fisher Scientific) according to the manufacturer instructions. Cultured hippocampal neurons were treated with 100 nM rapamycin (catalog #R0161, LKT Labs) or 2 μM lonafarnib (catalog # S2797, Selleck) for 7 d and fixed at DIV21.

Mouse cultured hippocampal neurons were fixed in 4% paraformaldehyde (PFA), blocked, permeabilized with BL solution (3% normal goat serum or 3% bovine serum albumin with 0.1% Triton X-100 in PBS), and incubated overnight at 4°C with one of the following primary antibodies: anti-GFP (chicken; 1:1000; catalog #AB16901, Merck Millipore) or anti-vesicular glutamate transporter 1 (VGluT1; guinea pig; 1:500; catalog #AB5905, Merck Millipore). Immunoreactivity was visualized using species-specific, fluorochrome-conjugated secondary antibodies. Spine and shaft synapse density analyses were performed as described previously (Yasuda et al., 2014; Sugiura et al., 2015). In brief, the relatively proximal region (~150 µm from soma) of one dendrite was chosen randomly, and its length was measured. The number of VGluT1 puncta on the spine and shaft synapses of the dendritic segments was determined by counting the number of VGluT1 puncta that partially overlapped the GFP^+ shaft or spines. Any VGluT1 puncta that did not touch a GFP^+ dendrite were not included. In addition, individual dendritic spines were manually traced, and the maximum length and head width of each dendritic spine and spine density were measured. All quantification were conducted using MetaMorph software (Molecular Devices). For the cumulative plot graphs, we counted the number of spines below a certain length or width and calculated the percentage of the total number of measured spines.

Immunoblotting and antibodies. HEK293 T cells, cultured hippocampal neurons, and mouse brains and livers were homogenized [40 mM Tris-HCl, pH 7.6, 1 mM EDTA, 1 mM EGTA, 0.1% Triton X-100, protease inhibitor cocktail tablet (Complete EDTA-free; catalog #11873580001, Roche) and 1 mM phenylmethanelsulfonyl fluoride (catalog #P7626, Sigma-Aldrich)] and centrifuged at 17,900 × *g* at 4°C. The resultant soluble and insoluble fractions were immunoblotted as described previously (Sugiura et al., 2015), and primary antibodies against FLAG (1:800; catalog #F3165, Sigma-Aldrich), Rheb1 [1:1000; catalog #MAB3426, R&D Systems (recognizing whole Rheb); 1:1000; catalog #13879; Cell Signaling Technology (preferably recognizing unfarnesylated Rheb)], α/β-tubulin (1:1000; catalog #2148, Cell Signaling Technology), phospho (p)-ERK1/2 (Thr202/Tyr204; 1:1000; catalog #9101, Cell Signaling Technology), ERK1/2 (1:1000; catalog #9102, Cell Signaling Technology), syntenin1 (1:400; catalog #sc-100336, Santa Cruz Biotechnology), p-S6 (Ser240/244; 1:1000; catalog #5364, Cell Signaling Technology), and S6 (1:1000; catalog #2317, Cell Signaling Technology), and HRP-conjugated secondary antibodies (1:6000; catalog #170–6515, BIO-RAD) were used.

Quantitative analysis of dendritic arc immunofluorescence. Cultured hippocampal neurons (DIV15) were treated with lonafarnib (2 μM) or DMSO and incubated for 3 d, and then were exposed to vehicle (H_2O) or 10 μM (*S*)-3,5-dihydroxyphenylglycine (DHPG) (catalog #120020, Abcam) for 60 min. The neurons were fixed with 4% PFA, and were stained with anti-activity-regulated cytoskeleton-associated protein (Arc; mouse; 1:25; catalog #sc-17839, Santa Cruz Biotechnology) and anti-microtubule-associated protein 2 (MAP2; rabbit; 1:500;

catalog #AB5622-I, Merck Millipore) antibodies as previously described (Sugiura et al., 2015). Images of stained neurons were collected with a confocal microscope (model LSM710, Carl Zeiss) with a 63× objective [numerical aperture (NA), 1.4]. Two-dimensional maximum projection images were reconstructed, and they were analyzed using MetaMorph software (Molecular Devices). The background corresponding to areas without cells was subtracted to make a "background-subtracted" image. Neurons were selected blindly based on the MAP2 fluorescence, and one dendrite was randomly chosen from one neuron. Twenty-micrometer-long regions along the dendrites (50–70 μm from soma) were manually outlined, and the average gray values (immunofluorescence integrated intensity) of each region were measured. The average value of H_2O-treated dendrites was defined as "base value," and each value of DHPG-treated dendrites was divided by the base value of each condition.

Contextual fear discrimination test. Eight- to 16-week-old mice were fear conditioned to the training context with three 0.1 mA shocks (2 s each) controlled by TimeFZ4 software (OHARA). Training sessions were 5 min in duration. Conditioned fear responses were assessed on the next day by TimeFZ4 software, which measured the percentage of time spent motionless during the test period (5 min session). To determine context-dependent conditioned responses, trained mice were assessed in the same training context and in a novel context (both were 5 min sessions). The novel context was created by varying the following conditions of the testing apparatus (training context vs novel context): room shape (rectangle vs triangle), wall opacity (clear vs opaque), floor material (metal bars vs plastic plate), lighting (150 vs 30 lux), and background white noise (65 vs 70 dB). All apparatus are manufactured by OHARA. For pharmacological experiments, the animals were orally administered lonafarnib (40 mg/kg) or vehicle [1% carboxymethyl cellulose (CMC; catalog #419273, Sigma-Aldrich), 0.9% NaCl, and 5% DMSO, 10 ml/kg].

Hot plate test. Eight- to 16-week-old mice were placed on a plate heated to 55 ± 0.5°C (model NPH-M30N, Nissin Rika). A square acryl tube was placed on the plate to prevent evacuation of the mouse. Nociception was assessed by measuring the latency time for licking the hindpaws or jumping (the cutoff time was 60 s).

Diolistic labeling. Eight- to 16-week-old mice were orally administered lonafarnib (40 mg/kg) or vehicle. On the next day, the mice were deeply anesthetized and perfused transcardially with PBS, followed by 4% PFA in 0.1 M phosphate buffer, pH 7.4. The brains were rapidly removed and postfixed for >24 h with 4% PFA; then, the brains were placed in PBS. Subsequently, 250-μm-thick coronal brain sections were obtained using a vibratome (model VT1200 S, Leica) and stored in PBS. Twenty-five milligrams of gold particles (catalog #1652263, BIO-RAD) was coated with 7.0 mg of the lipophilic dye DiI (catalog #D282, Thermo Fisher Scientific) and injected into Tefzel tubing, which was then cut into bullets. These particles were delivered diolistically at 80 psi using a Helios Gene Gun system (BIO-RAD). The slices were fixed again in 4% PFA for 15 min and mounted on slides in Vectashield Mounting Medium (catalog #H-1000, Vector Laboratories). Confocal images of dendrites were taken in stratum radiatum of CA1 domain. Each image was at least 100 μm apart, so one dendrite image should represent one neuron. Images were obtained with an confocal microscope (model LSM780, Carl Zeiss) using a 63× lens (Carl Zeiss; NA, 1.4) with sequential acquisition settings at the resolution of the confocal microscope (512 × 512 pixels). Three-dimensional stack images were acquired with the interval between images set to 0.407 μm. Stack images were maximally projected by the Zen program (Zeiss). Projected spine images were quantified with MetaMorph image analysis software (Molecular Devices) as follows: individual dendritic spines were manually traced, and the maximum length and head width of each dendritic spine and spine density were measured. For the cumulative plot graphs, we counted the number of spines below a certain length or width and calculated the percentage of the total number of measured spines.

Immunohistochemistry. To measure Arc levels, individual mice resting in their home cages during their daytime sleep cycle were rapidly anesthetized and perfused with 4% PFA; then, the tissues were incubated in sucrose and sectioned. To block nonspecific binding, brain sections were incubated in 5% goat and donkey serum for 2 h at room temperature. The sections were incubated for 3 d at 4°C in mouse anti-Arc antibody (1:100, Santa Cruz Biotechnology) diluted in a blocking solution. Biotinylated anti-mouse secondary antibody (1:1000; Vector Laboratories) was diluted in a manner similar to the primary antibody and applied to the sections for 2 h. An Avidin-Biotin Complex (ABC) Kit (Vector Laboratories) and 3,3-diaminobenzidine tetrahydrochloride (catalog # D5637, Sigma-Aldrich) were used to visualize antibody labeling. Sections were imaged and analyzed with AxioVision (Carl Zeiss). Arc immunoreactivity was quantified in the entire granular cell layer of the dentate gyrus (DG) in dorsal hippocampal sections (−1.82 to −1.34 mm bregma). To obtain high-resolution photomicrographs of the entire DG within a brain section, multiple images of each brain section were acquired and automatically reconstructed. Regions of interest representing individual cells were visualized and quantified to obtain the total number of Arc-immunoreactive cells and the total area per section. These values were averaged per mouse and compared across genotypes.

To measure S6 and phospho-S6 levels, mice were orally administered lonafarnib (40 mg/kg) or vehicle. On the next day, the mice were deeply anesthetized and perfused transcardially with PBS, followed by 4% PFA in 0.1 M phosphate buffer, pH 7.4. The brains were rapidly removed and postfixed for >24 h with 4% PFA; then, the tissues were incubated in 20% sucrose for >20 h and sectioned by 30 μm thickness. Antigen retrieval was performed by a heat-induced epitope retrieval technique using microwave oven. In brief, brain sections were immersed in 10 mM sodium citrate buffer, pH 6.0, and boiled for 5 min, three times (10 min interval). Slides were cooled to room temperature for 30 min and washed with PBS for 10 min, three times. To block nonspecific binding, brain sections were incubated in PBS with 2% goat serum 0.1% Triton X-100 for 2 h at room temperature. The sections were incubated for 5 d at 4°C in anti-S6 antibody (1:50; catalog #2317, Cell Signaling Technology) and anti-phospho-S6 antibody (Ser240/244; 1:800; catalog #5364, Cell Signaling Technology) diluted in a blocking solution. Immunoreactivity was visualized using species-specific, Alexa Fluor 488- or Alexa Fluor 568-conjugated secondary antibodies (1:1000; Thermo Fisher Scientific). Secondary antibodies were diluted in PBS with 0.1% Triton X-100 applied to the sections for 2 h at room temperature. Sections were imaged with AxioImager Z.1 with the MosaiX option (Carl Zeiss). S6 and p-S6 immunoreactivity was quantified in the entire granular cell layer of the dentate gyrus images in dorsal hippocampal sections (−1.82 to −1.34 mm from bregma). MetaMorph software was used for the quantification. The whole granular cell layer was selected, and the averages of S6 and p-S6 intensity of the selected area were collected. The background intensity was collected from the area of the ventricle, and background intensity was subtracted from the granular cell layer intensity. The calculated p-S6 intensity was divided by the calculated S6 intensity, and the result was treated as the p-S6/S6 intensity value.

Experimental design and statistical analysis. GraphPad Prism version 8.0 software was used for statistical analyses of the data. Detailed methods are described in the figure legends. Differences were considered significant at $p < 0.05$. All experiments requiring the use of animals, directly or as a source of cells, were subjected to randomization.

Results

Farnesylation inhibition restored dendritic spine formation in *Tsc2*$^{+/-}$ mouse hippocampal neurons

We reported that *Tsc2*$^{+/-}$ rat neurons showed impaired synapse formation, including reduced spine synapses or increased shaft synapses (Sugiura et al., 2015). To assess the efficacy of FTIs for the treatment of synaptic abnormalities in TSC mouse neurons, we tested whether FTI treatment restores proper synapse formation in cultured *Tsc2*$^{+/-}$ mouse neurons. Treatment with the FTI lonafarnib (SCH66336) increased the dendritic spine width and decreased the spine length of *Tsc2*$^{+/-}$ mouse neurons (Fig. 1*a*,*b*). Lonafarnib treatment almost completely restored spine synapse formation in *Tsc2*$^{+/-}$ mouse neurons, whereas spine density was not altered by lonafarnib treatment (Fig. 1*a*,*c*,*d*). In contrast, treatment with the mTORC1 inhibitor rapamycin did

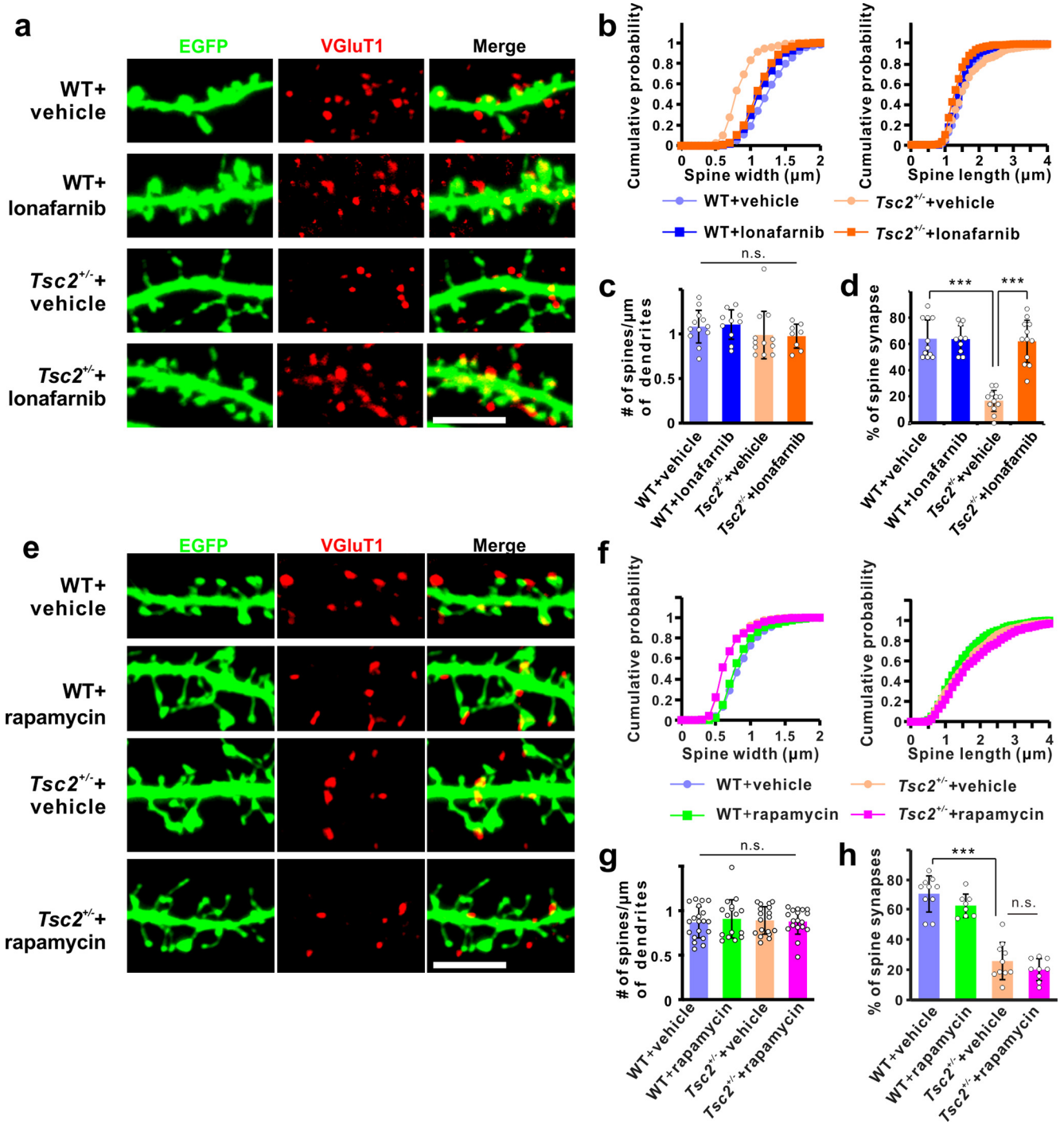

Figure 1. Treatment with FTIs and heterozygous knockout of Rheb1 restored spine synapse formation in $Tsc2^{+/-}$ neurons. ***a***, Confocal images of EGFP-expressing cultured hippocampal neurons from WT or $Tsc2^{+/-}$ mouse. Immunodetection of $VGluT1^{+}$ (red) presynaptic boutons on EGFP (green)-expressing WT and $Tsc2^{+/-}$ neurons treated with DMSO (vehicle) or 2 μM lonafarnib. Scale bar, 5 μm. ***b***, Cumulative probability distributions of the spine widths (left) and lengths (right) in ***a***. Note that lonafarnib treatment increased the dendritic spine width (D = 0.5180; $^{***}p < 0.0001$) and decreased the dendritic spine length (D = 0.247; $^{***}p < 0.001$) compared with vehicle treatment in $Tsc2^{+/-}$ neurons [spines/neurons, respectively; $n = 541/12$ (WT/vehicle), $n = 363/10$ (WT/lonafarnib), $n = 525/12$ ($Tsc2^{+/-}$/vehicle), and $n = 328/8$ ($Tsc2^{+/-}$/lonafarnib)]. ***c***, No significant differences were observed in spine density in the condition of ***a*** [dendrites; $n = 12$ (WT, vehicle), $n = 10$ (WT, lonafarnib), $n = 12$ ($Tsc2^{+/-}$, vehicle), and $n = 8$ ($Tsc2^{+/-}$, lonafarnib); one-way ANOVA: $F_{(3,38)} = 0.996$, $p = 0.405$; two-way ANOVA: treatment × genotype interaction: $F_{(1,38)} = 0.078$, $p = 0.781$; genotype: $F_{(1,38)} = 2.948$, $p = 0.094$; treatment: $F_{(1,38)} = 0.008$, $p = 0.931$]. ***d***, Quantification of $VGluT1^{+}$ spines in ***a***. The decrease of spine synapses in $Tsc2^{+/-}$ was recovered by lonafarnib treatment [dendrites; $n = 11$ (WT, vehicle), $n = 10$ (WT, lonafarnib), $n = 12$ ($Tsc2^{+/-}$, vehicle), and $n = 12$ ($Tsc2^{+/-}$, lonafarnib); one-way ANOVA, *post hoc* Tukey's test, $F_{(3,41)} = 36.13$; $^{***}p < 0.001$, $Tsc2^{+/-}$ + vehicle vs WT + vehicle; $^{***}p < 0.001$, $Tsc2^{+/-}$ + vehicle vs $Tsc2^{+/-}$ + lonafarnib; two-way ANOVA: treatment × genotype interaction: $F_{(1,41)} = 32.93$, $p < 0.001$; genotype: $F_{(1,41)} = 38.15$, $p < 0.001$; treatment: $F_{(1,41)} = 32.50$, $p < 0.001$]. ***e***, Confocal images of EGFP-expressing cultured hippocampal neurons from a WT or $Tsc2^{+/-}$ mouse. Immunodetection of $VGluT1^{+}$ (red) presynaptic boutons on EGFP (green)-expressing WT and $Tsc2^{+/-}$ neurons treated with DMSO (vehicle) or 100 nM rapamycin. Scale bar, 5 μm. ***f***, Cumulative probability plots of the dendritic spine widths (left) and lengths (right) in ***e***. Note that rapamycin treatment increased the dendritic spine length (D = 0.086, $^{*}p = 0.030$) and did not alter the dendritic spine width (D = 0.028, $p = 0.982$) compared with those following DMSO treatment in $Tsc2^{+/-}$ neurons [spines/neurons, respectively; $n = 570/20$ (WT/vehicle), $n = 564/17$ (WT/rapamycin), $n = 579/18$ ($Tsc2^{+/-}$/vehicle), and $n = 551/18$ ($Tsc2^{+/-}$/rapamycin); Kolmogorov–Smirnov test]. ***g***, No significant differences were observed in spine density in the condition of ***e*** [dendrites; $n = 20$ (WT, vehicle), $n = 17$ (WT, rapamycin), $n = 18$ ($Tsc2^{+/-}$, vehicle), and $n = 18$ ($Tsc2^{+/-}$, rapamycin); one-way ANOVA:

not affect the spine width, length, or spine synapse ratio in either wild-type (WT) or *Tsc2*$^{+/-}$ mouse neurons (Fig. 1*e–h*). Thus, pharmacological inhibition of Rheb1, but not mTORC1, may rescue proper synapse formation in *Tsc2*$^{+/-}$ neurons.

Lonafarnib suppressed the activation of Rheb1 but not Ras

We next sought to corroborate biochemical inhibition of Rheb1 farnesylation in FTI-treated neurons. FLAG-Rheb1 was expressed in HEK293 T cells, which were then treated with 2 μM lonafarnib or DMSO for 24 h. The treated cells were fractionated into soluble and insoluble fractions and immunoblotted with an anti-FLAG antibody. We estimated the farnesylation status of Rheb1 by a mobility shift assay; the farnesylated Rheb1 protein migrates faster in SDS-PAGE gels than unfarnesylated Rheb1 (Basso et al., 2005), and also unfarnesylated Rheb1 migrates slower than the nonfarnesylated Rheb1 mutant does (Wang et al., 2008). Lonafarnib treatment slowed the movement of the soluble FLAG-Rheb1 protein, suggesting that most soluble Rheb1 was unfarnesylated in the lonafarnib-treated cells (Fig. 2*a*). Among the insoluble fractions, a small amount of farnesylated Rheb1 remained in the untreated cells, but none was detected in the lonafarnib-treated cells (Fig. 2*a*; Clark et al., 1997). Thus, FTI treatment may increase unfarnesylated Rheb1 protein levels; however, total Rheb1 protein levels were reduced in lonafarnib-treated cells, probably via protein degradation (Sugiura et al., 2015).

To evaluate whether the endogenous Rheb1 protein is also affected by FTI treatment, we treated HEK293 T cells with lonafarnib or DMSO, and immunoblotted their extracts with anti-Rheb1 antibody. Again, the Rheb1 protein in lonafarnib-treated cells migrated more slowly than that in DMSO-treated cells (Fig. 2*b*). Then, we tested the effects of lonafarnib on the neuronal Rheb1 protein. We cultured hippocampal neurons from wild-type mice and treated them with 2 μM lonafarnib or DMSO for 24 h; however, we did not see any difference in the size of the Rheb1 protein between DMSO- and lonafarnib-treated cells with the same antibody. This may be because the mobility shift of farnesylated Rheb1 in mouse cells is not easily visualized because of close proximity. Therefore, we used the antibody that mainly recognized the unfarnesylated Rheb1 protein, and observed lonafarnib treatment caused a robust increase in unfarnesylated Rheb1 levels compared with those following DMSO treatment (Fig. 2*c*), indicating that lonafarnib treatment clearly upregulates unfarnesylated Rheb1 levels in cultured neurons.

FTIs may also act through the inhibition of mTORC1 signaling following the unfarnesylation of Rheb1. Therefore, we immunoblotted vehicle- or lonafarnib-treated neuronal lysates with anti-phospho S6 antibody. However, lonafarnib treatment did not affect S6 phosphorylation in cultured hippocampal neurons under our conditions (2 μM lonafarnib for 24 h; Fig. 2*d*). Previous literature shows that 1 μM lonafarnib treatment almost completely suppressed the phosphorylation of S6 in MCF cells (a human breast cancer cell line; Basso et al., 2005). This discrepancy could be because of cell type specificity (primary neurons vs breast cancer cells). mTORC1 signaling may be activated in cancer cells through Rheb1, whereas amino acid–Rag signaling might play more crucial roles in neuronal mTOR regulation. In fact, several RAG1-GAP mutations cause dysplasia in only the brain, but not in other organs, via the activation of mTORC1 (Iffland et al., 2019). Thus, the inhibition of Rheb1 farnesylation could have a less substantial effect on mTORC1 activity in neurons than in other cell types. Our result may also be in line with the observation that lovastatin, which also blocks protein prenylation, did not reduce the phosphorylation of S6 kinase or the S6 protein in hippocampal slices (Osterweil et al., 2013). FTIs may exert their effects via another pathway distinct from mTORC1 signaling.

FTIs inhibit the farnesylation of other signaling molecules, such as Ras. To test whether the effects of lonafarnib on TSC neurons were because of the inhibition of Ras function, we examined the phosphorylation status of ERK1/2, which is a downstream kinase of H-Ras signaling (Osterweil et al., 2013). However, we failed to detect any inhibition of ERK1/2 phosphorylation in lonafarnib-treated cultured neurons (Fig. 2*e*). Thus, Ras inhibition does not seem to be involved in the neuronal mechanism of lonafarnib action. This may be because the Ras protein can be alternatively prenylated by geranylgeranyl transferase-1 in the presence of an FTI (Whyte et al., 1997). These results suggest that **the** inhibition of Rheb1 may normalize synaptic abnormalities in *Tsc2*$^{+/-}$ neurons in an mTORC1- or MAPK-independent manner.

Finally, we investigated the time required for lonafarnib to accumulate unfarnesylated Rheb1. We treated HEK293 T cells with lonafarnib, and collected their extracts at the indicated time point. Unfarnesylated Rheb1 could be detected 3 h after lonafarnib treatment, and a significant increase could be observed 6 h after the addition of lonafarnib (Fig. 2*f*). A gradual increase of unfarnesylated Rheb1 was observed thereafter. We assumed that it is better to wait at least 6 h after the administration of lonafarnib for additional experiments.

Lonafarnib treatment decreased Rheb1 protein levels in a syntenin-dependent manner

We previously demonstrated that Rheb1 activation released the PDZ protein syntenin, which bound syndecan-2 to impair synapse formation, in *Tsc2*$^{+/-}$ neurons (Sugiura et al., 2015). We therefore assessed whether Rheb1–syntenin signaling (Sugiura et al., 2015) is involved in FTI-induced Rheb1 suppression. FLAG-Rheb1 was expressed with or without EGFP-syntenin in HEK293 T cells. The cells were then incubated with 2 μM lonafarnib for 24 h, along with 20 μM MG-132 or DMSO during the last 6 h. Unfarnesylated FLAG-Rheb1 levels were compared between the presence and absence of syntenin. Compared with the absence of syntenin, the coexpression of syntenin significantly reduced unfarnesylated Rheb1 levels in lonafarnib-treated cells (Fig. 2*g*). We have shown that the unfarnesylated Rheb1–syntenin complex appeared to be degraded by proteasome (Sugiura et al., 2015). Therefore, we treated the syntenin-expressing cell with a proteasome inhibitor, MG-132, and found that the unfarnesylated Rheb1 levels are not reduced in the presence of MG-132. Thus, lonafarnib could reduce the Rheb1 levels by increasing the

←

$F_{(3,69)} = 0.167$, $p = 0.919$; two-way ANOVA: treatment × genotype interaction: $F_{(1,69)} = 0.381$, $p = 0.539$; genotype: $F_{(1,69)} = 0.009$, $p = 0.924$; treatment: $F_{(1,69)} = 0.111$, $p = 0.741$]. ***h***, Quantification of VGluT1$^+$ spines in ***e***. Rapamycin treatment did not alter the decrease of spine synapses in *Tsc2*$^{+/-}$ neurons [dendrites; $n = 10$ (WT, vehicle), $n = 8$ (WT, rapamycin), $n = 10$ (*Tsc2*$^{+/-}$, vehicle), and $n = 9$ (*Tsc2*$^{+/-}$, rapamycin); one-way ANOVA, *post hoc* Tukey's test: $F_{(3,33)} = 56.93$; ***$p < 0.001$, *Tsc2*$^{+/-}$ + vehicle vs WT + vehicle; $p = 0.628$, *Tsc2*$^{+/-}$ + vehicle vs *Tsc2*$^{+/-}$ + rapamycin; two-way ANOVA: treatment × genotype interaction: $F_{(1,33)} = 0.094$, $p = 0.761$; genotype: $F_{(1,33)} = 163.4$, $p < 0.001$; treatment: $F_{(1,33)} = 3.931$, $p = 0.056$]. Error bars indicate SD. ***$p < 0.005$, n.s.: not significant. D: the largest absolute difference between the two distribution functions across all values.

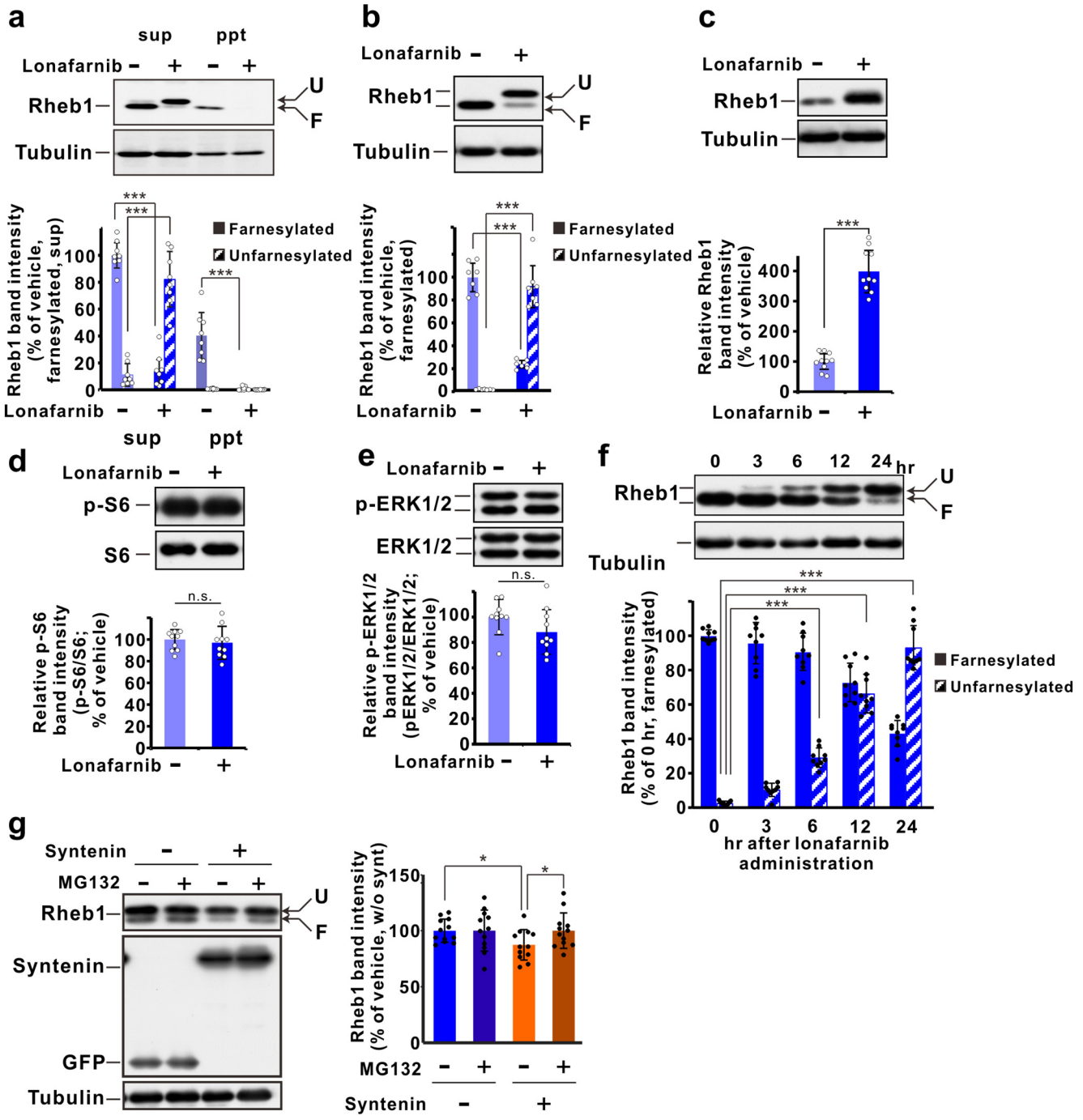

Figure 2. Rheb1 farnesylation and protein levels were modified by lonafarnib treatment. ***a***, SDS-PAGE analyses of Rheb1 farnesylation. HEK293 T cells transfected with FLAG-Rheb1 were incubated with DMSO (lanes 1 and 3) or 2 μM lonafarnib (lanes 2 and 4), and their lysates were separated into supernatant (sup) and pellet (ppt) fractions. Top, Unfarnesylated (U) and farnesylated (F) FLAG-Rheb1 proteins are indicated. Bottom, Quantification of unfarnesylated and farnesylated FLAG-Rheb1 proteins in each fraction shown in the top panel ($n = 8$ independent experiments; two-tailed t test with Welch's correction: $t_{(13.84)} = 15.090$, $^{***}p < 0.001$, vehicle-treated condition vs lonafarnib-treated condition in sup-farnesylated; $t_{(9.182)} = 9.030$, $^{***}p < 0.001$, vehicle-treated condition vs lonafarnib-treated condition in sup-unfarnesylated; and $t_{(7.084)} = 6.374$, $^{***}p < 0.001$ vehicle-treated condition vs lonafarnib-treated ppt-farnesylated; three-way ANOVA: solubility × treatment × farnesylation interaction: $F_{(1,56)} = 105.1$, $p < 0.001$; solubility × treatment interaction: $F_{(1,56)} = 4.895$, $p = 0.031$; solubility × farnesylation interaction: $F_{(1,56)} = 2.711$, $p = 0.105$; treatment × farnesylation interaction: $F_{(1,56)} = 288.8$, $p < 0.001$; solubility: $F_{(1,56)} = 207.6$, $p < 0.001$; treatment: $F_{(1,56)} = 22.35$, $p < 0.001$; farnesylation: $F_{(1,56)} = 29.14$, $p < 0.001$. ***b***, Top, Lonafarnib treatment also increased unfarnesylation of endogenous Rheb1 protein in HEK293 T cells. Bottom, Quantification of unfarnesylated and farnesylated Rheb1 proteins in each homogenate shown in the top panel ($n = 7$ independent experiments, two-tailed t test with Welch's correction: $t_{(6.829)} = 14.394$, $^{***}p < 0.001$, vehicle-treated condition vs lonafarnib-treated condition farnesylated; $t_{(6.004)} = 11.953$, $^{***}p < 0.001$, vehicle-treated condition vs lonafarnib-treated condition unfarnesylated; two-way ANOVA: treatment × farnesylation interaction: $F_{(1,24)} = 326.2$, $p < 0.001$; treatment: $F_{(1,24)} = 2.204$, $p = 0.151$; farnesylation: $F_{(1,24)} = 10.56$, $p = 0.003$). ***c***, Top, Lonafarnib treatment drastically increased unfarnesylated Rheb1 levels in primary cultured hippocampal neurons. Bottom, Quantification of Rheb1 levels in each homogenate shown in the top panel ($n = 7$ independent experiments, two-tailed t test with Welch's correction: $t_{(11.943)} = 12.186$, $^{***}p < 0.001$). ***d***, Lonafarnib did not influence the activation of mTORC1. Primary cultured hippocampal neurons were treated with DMSO or lonafarnib. Top, p-S6 levels in each supernatant were compared. Bottom, Quantification of the p-S6 levels in each homogenate shown in the top panel ($n = 10$ independent experiments; two-tailed t test with Welch's correction, $t_{(15.620)} = 0.529$ $p = 0.604$). ***e***, Lonafarnib did not affect the activation of ERK1/2. Top, Primary cultured hippocampal neurons were treated with DMSO or lonafarnib. Phospho-ERK1/2 levels in each supernatant were compared. Bottom, Quantification of phospho-ERK1/2 levels in each homogenate shown in the top panel

unfarnesylated Rheb1, which might be prone to syntenin-dependent degradation.

Lonafarnib treatment increased unfarnesylated Rheb1 and restored synaptic morphology in the brain

To evaluate whether lonafarnib increases unfarnesylated Rheb1 in the brain, we administered lonafarnib (40 mg/kg) or vehicle to adult wild-type mice and dissected and extracted their livers and hippocampi 6 h later. Each soluble fraction was separated by SDS-PAGE and immunoblotted with anti-Rheb1 antibody. Lonafarnib treatment clearly increased unfarnesylated Rheb1 levels in the liver but not in the hippocampus (Fig. 3*a*,*b*). Because basal levels of unfarnesylated Rheb1 are higher in the hippocampus than in the liver, a small increase in Rheb1 level in the hippocampus might be less obvious than that in the liver. Therefore, we examined another farnesylated protein, HDJ2, instead of Rheb1 and detected a significant increase in mobility-shifted HDJ2 protein in the hippocampi of lonafarnib-treated mice compared with vehicle-treated mice (Fig. 3*c*). In contrast, phosphorylation of the S6 protein and MAP kinase was no different in the brains of vehicle- and lonafarnib-treated mice (Fig. 3*d*,*e*). Immunohistochemistry also showed that phosphorylation of S6 protein did not change by lonafarnib treatment (Fig. 3*f*,*g*).

Next, to examine synaptic recovery by the FTI in the brain, we labeled hippocampal CA1 neurons in hippocampal slices prepared from vehicle- or lonafarnib-treated WT and $Tsc2^{+/-}$ mouse brains with biolistic-DiI. Vehicle or lonafarnib was administered on the day before perfusion. The dendritic spines in vehicle-treated $Tsc2^{+/-}$ neurons were significantly thinner than those in WT neurons; however, the spine length did not show a significant difference between WT and $Tsc2^{+/-}$ mice, inconsistent with the results of neuronal cultures (Fig. 1*b*). This might be because of the difference in the surrounding environment; that is, sparse cultured neurons may more easily elongate and form dendritic spines than those in the brain, enhancing the difference in length. Lonafarnib treatment increased spine widths, but not spine density, in $Tsc2^{+/-}$ neurons to a similar extent as WT neurons (Fig. 3*h*–*j*), suggesting that lonafarnib reaches the hippocampus through the blood–brain barrier and may restore synaptic morphology via an increase in the unfarnesylated Rheb1 protein in the neurons.

Farnesylation inhibition restored memory deficits in $Tsc2^{+/-}$ mice

A previous study showed that $Tsc2^{+/-}$ mice have an impaired ability to distinguish between familiar and novel contexts in a fear-conditioning task (Ehninger et al., 2008). Because lonafarnib restored synaptic morphology (Figs. 1, 3), we tested whether the FTI ameliorates cognitive deficits in $Tsc2^{+/-}$ mice. For this behavioral test, mice are exposed to a footshock. The next day, contextual discrimination is tested by measuring the freezing time in the original context and in a distinct context. Before this discrimination test, we compared the pain thresholds of WT and $Tsc2^{+/-}$ mice by the hot plate test, but we did not find any significant difference in pain threshold between the genotypes (Fig. 4*a*). For fear discrimination, WT mice that were orally administered vehicle could distinguish the contexts, whereas the vehicle-treated $Tsc2^{+/-}$ mice could not (Fig. 4*b*). The oral administration of lonafarnib (40 mg/kg) 6 h before training eliminated the lack of context discrimination in $Tsc2^{+/-}$ mice (Fig. 4*b*). Thus, the administration of lonafarnib before footshock (encoding) restored contextual memory in $Tsc2^{+/-}$ mice. Next, to determine whether lonafarnib treatment after learning also improves memory retrieval, we administered lonafarnib to $Tsc2^{+/-}$ mice after footshock (6 h before recall). However, these $Tsc2^{+/-}$ mice could not discriminate different contexts (Fig. 4*c*), suggesting that the administration of lonafarnib before learning (encoding) is required in $Tsc2^{+/-}$ mice during the learning phase to rescue the learning defect. Interestingly, it was not significant, but the administration of lonafarnib to $Tsc2^{+/-}$ mice increased the freezing time in the original context, whereas the freezing time in distinct context was affected by whether lonafarnib was administrated before or after the footshock. These results suggest that $Tsc2^{+/-}$ mice show a disability in memory encoding rather than memory retrieval, and that lonafarnib shows the efficacy to restore the synaptic encoding that may be required during the memory retrieval.

The DHPG-induced increase in dendritic arc protein levels was reversed in $Tsc2^{+/-}$ neurons by lonafarnib treatment

Several lines of evidence show that long-term depression (LTD) induced by the metabotropic glutamate receptor (mGluR)-selective agonist DHPG is impaired in mouse models of TSC (Auerbach et al., 2011; Bateup et al., 2011). In particular, Auerbach et al. (2011) demonstrated that a decrease in the translation of Arc caused mGluR-LTD suppression in TSC mice. Arc stimulates the trafficking of AMPA receptors and induces mGluR-LTD (Chowdhury et al., 2006; Waung et al., 2008). Therefore, we compared the DHPG-induced increase in dendritic Arc levels between cultured WT and $Tsc2^{+/-}$ neurons. In WT neurons, DHPG stimulation significantly increased dendritic Arc levels compared with basal levels (Fig. 5*a*–*c*). However, DHPG treatment did not increase dendritic Arc levels in $Tsc2^{+/-}$ neurons (Fig. 5*b*,*c*). Prior treatment of $Tsc2^{+/-}$ neurons with lonafarnib restored the DHPG-induced increase in dendritic Arc levels (Fig. 5*b*,*c*). Together, FTI treatment recovered DHPG-mediated dendritic Arc expression in TSC neurons, suggesting that the FTI-dependent increase of Arc expression could restore the mGluR-LTD impairment in TSC mice.

Lonafarnib treatment restored activity-regulated Arc expression by memory retrieval in the hippocampus

To verify restoration of activity-regulated plastic change in $Tsc2^{+/-}$ mice, we examined Arc expression in the hippocampus *in vivo*. Arc is involved in spatial memory formation (Guzowski

←

($n = 10$ independent experiments, two-tailed t test with Welch's correction: $t_{(16.410)} = 1.674$, $p = 0.113$). ***f***, Left, Six hours of lonafarnib treatment was sufficient to increase unfarnesylated Rheb1 in HEK293 T cells. Right, Quantification of unfarnesylated and farnesylated Rheb1 proteins in each homogenate shown in the top panel [$n = 9$ independent experiments, *post hoc* Dunnett's test: $F_{(4,40)} = 196.495$; ***$p < 0.001$ (0 h vs 6, 12, and 24 h); $p = 0.160$ (0 vs 3 h); two-way ANOVA: time point × farnesylation interaction: $F_{(4,80)} = 213.0$, $p < 0.001$; time point: $F_{(4,80)} = 16.02$, $p < 0.001$; farnesylation: $F_{(1,80)} = 458.7$, $p < 0.001$]. ***g***, Lonafarnib treatment decreased unfarnesylated Rheb1 levels in a syntenin-dependent manner. Top, HEK293 T cells transfected with FLAG-Rheb1 and with mock or EGFP-syntenin were incubated with lonafarnib and either DMSO (lanes 1 and 3) or MG132 (lanes 2 and 4). Bottom, Quantification of unfarnesylated Rheb1 proteins in each homogenate shown in the left panel ($n = 12$ independent experiments, two-tailed t test with Welch's correction: $t_{(20.516)} = 2.547$, *$p = 0.019$, vehicle-treated groups, syntenin (−) and syntenin (+) conditions; $t_{(21.511)} = 2.105$, *$p = 0.047$, syntenin (+) groups, vehicle-treated vs MG132-treated conditions; two-way ANOVA, treatment × syntenin interaction: $F_{(1,44)} = 2.154$, $p = 0.149$; treatment: $F_{(1,44)} = 2.231$, $p = 0.142$; syntenin: $F_{(1,44)} = 2.168$, $p = 0.148$). Error bars indicate SD. *$p < 0.05$, ***$p < 0.005$, n.s.: not significant. sup: supernatant, ppt: precipitate.

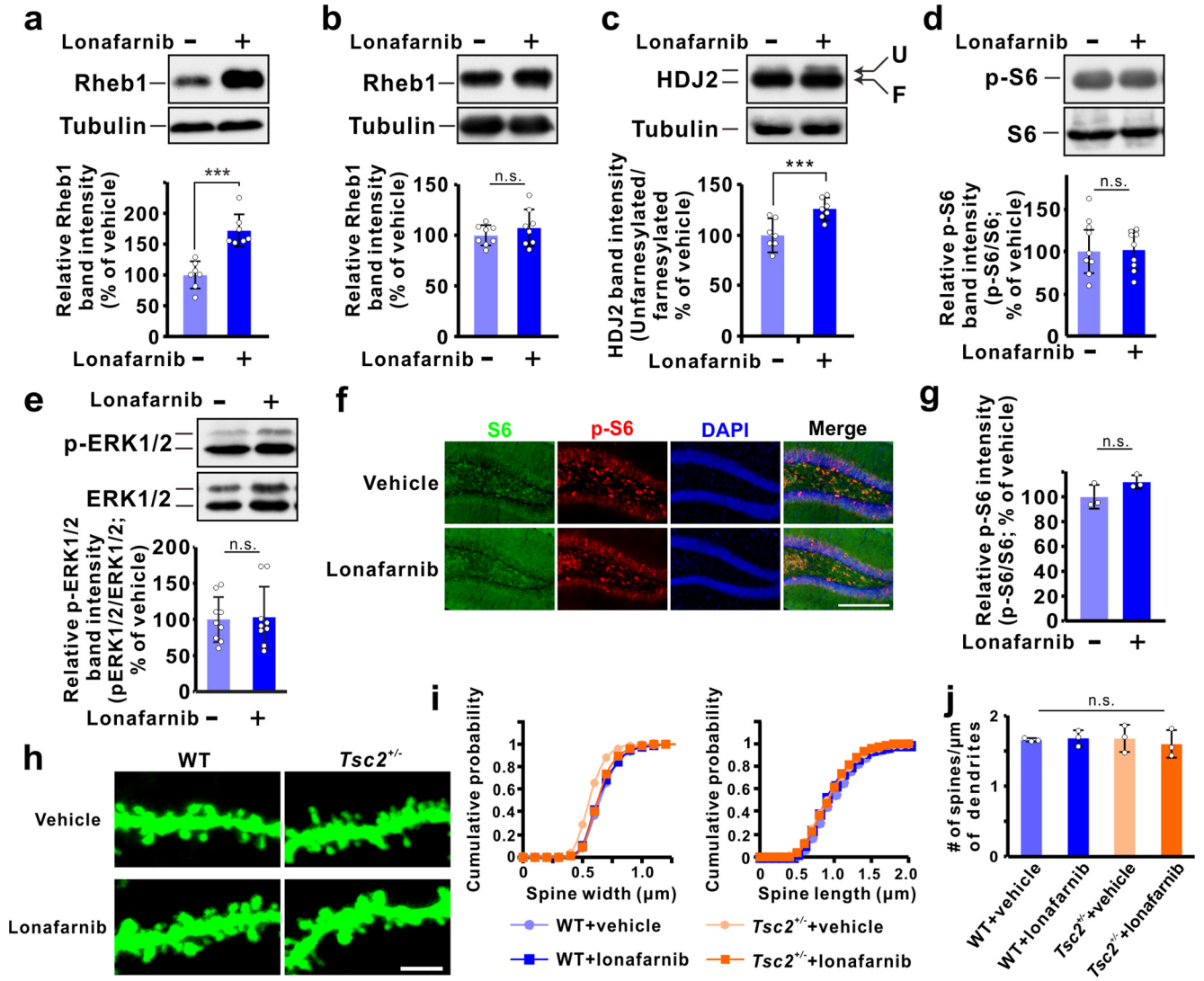

Figure 3. Lonafarnib treatment inhibited the farnesylation of a hippocampal protein and restored dendritic spine morphology in the hippocampi of $Tsc2^{+/-}$ mice *in vivo*. ***a***, Lonafarnib treatment increased unfarnesylated Rheb1 protein in the liver *in vivo*. Livers were dissected from WT mice treated with DMSO or lonafarnib. Top, Lonafarnib treatment drastically increased unfarnesylated Rheb1 levels. Bottom, Quantification of Rheb1 levels in each homogenate shown in the top panel ($n = 7$ independent experiments; two-tailed *t* test with Welch's correction: $t_{(11.659)} = 5.576$, $^{***}p < 0.001$). ***b***, Lonafarnib treatment did not show a significant increase in unfarnesylated Rheb1 levels in the hippocampus *in vivo*. Top, Hippocampi were dissected from WT mice treated with DMSO or lonafarnib. Bottom, Quantification of Rheb1 levels in each homogenate shown in the top panel ($n = 8$ independent experiments, two-tailed *t* test with Welch's correction: $t_{(10.950)} = 1.020$, $p = 0.330$). ***c***, Lonafarnib treatment increased unfarnesylated HDJ-2 protein in the hippocampus *in vivo*. Top, Hippocampi were dissected from WT mice treated with DMSO or lonafarnib. The HDJ-2 protein in each homogenate was immunoblotted. Unfarnesylated (U) and farnesylated (F) HDJ-2 proteins are indicated. Bottom, Quantification of the unfarnesylated HDJ-2 protein levels shown in the top panel ($n = 7$ independent experiments, two-tailed *t* test with Welch's correction: $t_{(10.860)} = 3.795$; $^{***}p = 0.003$). ***d***, Lonafarnib treatment did not affect p-S6 protein levels in the brain. Top, Phosphorylated and total S6 proteins are indicated. Bottom, Quantification of the phospho-S6 levels shown in the top panel ($n = 9$ independent experiments; two-tailed *t* test with Welch's correction: $t_{(14.326)} = 0.376$, $p = 0.713$). ***e***, Lonafarnib treatment did not affect the phosphorylation of MAP kinase in the brain. Top, Phosphorylated and total ERK1/2 proteins are indicated. Bottom, Quantification of the phospho-ERK1/2 levels shown in the top panel ($n = 9$ independent experiments; two-tailed *t* test with Welch's correction: $t_{(14.679)} = 0.169$, $p = 0.868$). ***f***, Representative images of S6 (green) and p-S6 (red) staining in the DG of vehicle- or lonafarnib-administered WT mice. Scale bar, 300 μm. ***g***, Quantification of relative p-S6/S6 intensity in the DG. Lonafarnib administration did not alter p-S6/S6 value in WT mice ($n = 18/3$ hippocampi/animals; two-tailed *t* test with Welch's correction: $t_{(3.13153)} = 1.899$, $p = 0.150$). Data are averaged and presented by mice. ***h***, Representative DiI-labeled dendrites from the hippocampal CA1 neurons of WT and $Tsc2^{+/-}$ mice treated with lonafarnib or vehicle. Scale bar, 2 μm. ***i***, Cumulative probability plots of the spine width (left) and spine length (right) in ***h***. $Tsc2^{+/-}$ neurons showed a decreased spine width [$D = 0.316$; $^{***}p < 0.001$ ($Tsc2^{+/-}$ + vehicle vs WT + vehicle)], and lonafarnib treatment rescued the aberrant spine shape [$D = 0.2590$, $^{***}p < 0.001$, $Tsc2^{+/-}$ + vehicle vs $Tsc2^{+/-}$ + lonafarnib; spines/neurons/animals, respectively: $n = 1055/31/3$ (WT + vehicle), $n = 1155/30/3$ (WT + lonafarnib), $n = 1092/30/3$ ($Tsc2^{+/-}$ + vehicle), and $n = 1039/32/3$ ($Tsc2^{+/-}$ + lonafarnib); Kolmogorov–Smirnov test]. ***j***, Quantification of spine density in ***f*** [neurons/animals, respectively: $n = 31/3$ (WT, vehicle), 30/3 (WT, lonafarnib), $n = 30/3$ ($Tsc2^{+/-}$, vehicle), and $n = 32/3$ ($Tsc2^{+/-}$, lonafarnib); one-way ANOVA, $F_{(3,8)} = 0.195$ $p = 0.897$; two-way ANOVA: treatment × genotype interaction: $F_{(1,8)} = 0.361$, $p = 0.565$; genotype: $F_{(1,8)} = 0.098$, $p = 0.763$; treatment: $F_{(1,8)} = 0.126$, $p = 0.732$]. Data are averaged and presented by mouse type. Error bars indicate SD. $^{***}p < 0.005$, n.s.: not significant. D: the largest absolute difference between the two distribution functions across all values.

et al., 2001) and has been thought to reflect the regional specificity of space encoding using neuronal ensemble recordings (Vazdarjanova and Guzowski, 2004). Therefore, we compared the number of Arc-expressing neurons in the hippocampal DG between WT and $Tsc2^{+/-}$ mice, when they generate contextual memory recall (Fig. 6*a*). As a basal control, WT and $Tsc2^{+/-}$ mice were killed in their home cages (basal), and these mice had some basal Arc^{+} neurons in their DGs (Fig. 6*b*). As a retrieval group, WT and $Tsc2^{+/-}$ mice first received a footshock and were then exposed to the same context 24 h later. Both vehicle- and lonafarnib-treated WT mice exhibited a clear increase in the number of Arc^{+} neurons in their DGs by fear memory retrieval,

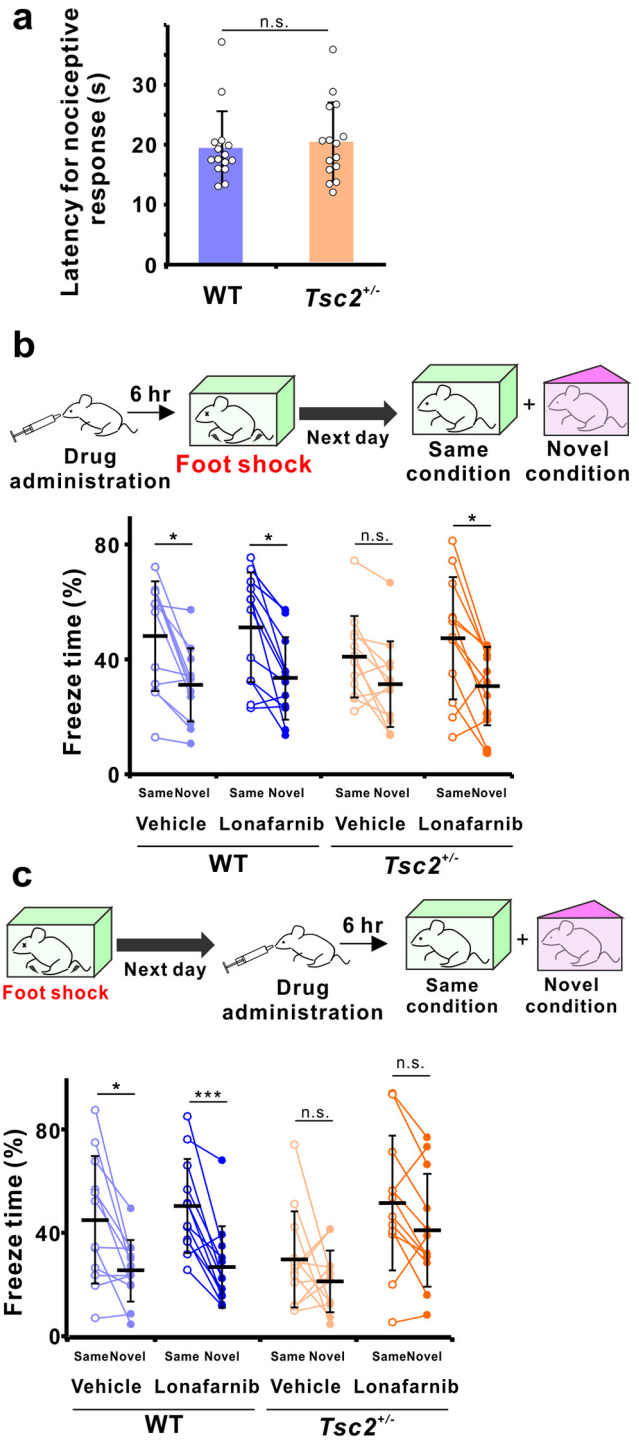

Figure 4. Lonafarnib treatment restored the fear memory deficits of *Tsc2*$^{+/-}$ mice in memory encoding. ***a***, The hot plate test indicated no significant difference in the time for a nociceptive response between WT and *Tsc2*$^{+/-}$ mice ($n = 15$ animals; two-tailed t test with Welch's correction: $t_{(27.861)} = 0.432$, $p = 0.669$). ***b***, Schematic illustration of the experimental design for the contextual learning task. Impaired contextual fear memory in *Tsc2*$^{+/-}$ mice was rescued by the oral administration of lonafarnib, whereas learning ability in WT mice was not altered by drug administration [$n = 12$ animals; two-tailed t test with Welch's correction: $t_{(19.247)} = 2.559$, $^{*}p = 0.019$ (WT + vehicle); $t_{(20.393)} = 2.546$, $^{*}p = 0.019$ (WT + lonafarnib); $t_{(21.978)} = 1.592$, $p = 0.126$ (*Tsc2*$^{+/-}$ + vehicle); $t_{(18.779)} = 2.341$, $^{*}p = 0.030$ (*Tsc2*$^{+/-}$ + lonafarnib); three-way ANOVA: genotype × treatment × apparatus interaction: $F_{(1,88)} = 0.280$, $p = 0.598$; genotype × treatment interaction: $F_{(1,88)} = 0.003$, $p = 0.954$; genotype × apparatus interaction: $F_{(1,88)} = 0.344$, $p = 0.559$; treatment × apparatus interaction: $F_{(1,88)} = 0.360$, $p = 0.550$; genotype: $F_{(1,88)} = 0.959$, $p = 0.330$; treatment: $F_{(1,88)} = 0.671$, $p = 0.415$; apparatus: $F_{(1,88)} = 20.68$, $p < 0.001$; multiple comparison after three-way ANOVA: *post hoc* Sidak's test, $p > 0.999$ (same: WT + vehicle vs WT + lonafarnib); $p > 0.999$ (novel: WT + vehicle vs WT + lonafarnib); $p = 0.990$ (same: *Tsc2*$^{+/-}$ + vehicle vs *Tsc2*$^{+/-}$ + lonafarnib); $p > 0.999$ (novel: *Tsc2*$^{+/-}$ + vehicle vs *Tsc2*$^{+/-}$ + lonafarnib)]. ***c***, Schematic illustration of the experimental design for the contextual learning task. Impaired contextual fear memory in *Tsc2*$^{+/-}$ mice was not rescued by the oral administration of lonafarnib after footshock, whereas the ability of the WT mice to learn was not altered by drug administration [$n = 12$ animals; two-tailed t test with Welch's correction: $t_{(15.876)} = 2.477$, $^{*}p = 0.025$ (WT + vehicle); $t_{(21.590)} = 3.386$, $^{***}p = 0.003$ (WT + lonafarnib); $t_{(18.761)} = 1.301$, $p = 0.209$ (*Tsc2*$^{+/-}$ + vehicle); $t_{(21.316)} = 1.076$, $p = 0.294$ (*Tsc2*$^{+/-}$ + lonafarnib); three-way ANOVA, genotype × treatment × apparatus interaction: $F_{(1,88)} = 0.011$, $p = 0.916$; genotype × treatment interaction: $F_{(1,88)} = 5.018$, $p = 0.028$; genotype × apparatus interaction: $F_{(1,88)} = 2.352$, $p = 0.129$; treatment × apparatus interaction: $F_{(1,88)} = 0.157$, $p = 0.693$; genotype: $F_{(1,88)} = 0.060$, $p = 0.806$; treatment: $F_{(1,88)} = 9.355$, $p = 0.003$; apparatus: $F_{(1,88)} = 15.47$, $p < 0.001$; multiple comparison after three-way ANOVA, *post hoc* Sidak's test: $p > 0.999$ (same: WT + vehicle vs WT + lonafarnib); $p > 0.999$ (novel: WT + vehicle vs WT + lonafarnib); $p = 0.074$ (same: *Tsc2*$^{+/-}$ + vehicle vs *Tsc2*$^{+/-}$ + lonafarnib); $p = 0.157$ (novel: *Tsc2*$^{+/-}$ + vehicle vs *Tsc2*$^{+/-}$ + lonafarnib); no outliers in the data, Grubb's test ($\alpha = 0.05$)]. Error bars indicate SD. $^{*}p < 0.05$, $^{***}p < 0.005$, n.s.: not significant.

whereas vehicle-treated *Tsc2*$^{+/-}$ mice did not (Fig. 6*b*,*c*). This suggests that when WT mice recall a memory, Arc may be induced in some populations of DG neurons, but this mechanism is impaired in *Tsc2*$^{+/-}$ mice. The oral administration of lonafarnib (40 mg/kg) 6 h before footshock significantly increased the number of Arc^{+} neurons in the *Tsc2*$^{+/-}$ mice after exposure to the same context. Thus, lonafarnib treatment may restore retrieval-related changes in Arc expression in *Tsc2*$^{+/-}$ mice by improving memory encoding, which is consistent with the findings that lonafarnib restored DHPG-induced Arc synthesis (Fig. 5) and memories (Fig. 4*b*) in *Tsc2*$^{+/-}$ neurons and mice, respectively. These results indicate that behavioral rescue by lonafarnib may be associated with restoration of the neural plasticity in the *Tsc2*$^{+/-}$ mice.

Heterozygous knockout of Rheb1 also restored synaptic abnormalities and contextual memory impairments in *Tsc2*$^{+/-}$ mice

Finally, in addition to pharmacological recovery, we validated that genetic reduction of Rheb1 is necessary for the restoration of synaptic abnormalities in *Tsc2*$^{+/-}$ neurons. We generated excitatory neuron-specific heterozygous *Rheb1* knock-out mice. Hippocampal neurons from *CamkII-Cre* (*Cre*), *CamkII-Cre; Rheb1*$^{flox/+}$ (*Rheb1-flox*), *Tsc2*$^{+/-}$*;CamkII-Cre* (*Tsc2*$^{+/-}$*;Cre*), and *Tsc2*$^{+/-}$*;CamkII-Cre;Rheb1*$^{flox/+}$ (*Tsc2*$^{+/-}$*; Rheb1-flox*) mice were cultured, and their spine morphologies were compared. Compared with *Cre* neurons, *Tsc2*$^{+/-}$*;Cre* neurons showed narrower and longer dendritic spines with a reduced spine synapse density. Heterozygous *Rheb1* knockout in *Tsc2*$^{+/-}$*;Cre* (*Tsc2*$^{+/-}$*; Rheb1-flox*) mice significantly increased the dendritic spine width/spine synapse ratio (Fig. 7*a–d*). Collectively, pharmacological and genetic inhibition of Rheb1 may rescue proper synapse formation in *Tsc2*$^{+/-}$ neurons.

We inferred that the inhibition of Rheb1 signaling benefits behavioral performance in *Tsc2*$^{+/-}$ mice. To further validate this hypothesis, we tested contextual discrimination in *Tsc2*$^{+/-}$*; Rheb1-flox* mice, based on the notion that excitatory neuron-specific *Rheb1* hetero-knockout mimics the reduced Rheb1 function with lonafarnib. *Tsc2*$^{+/-}$*; Rheb1-flox* mice recalled the context and froze longer than *Tsc2*$^{+/-}$*;Cre* mice with an equivalent pain sensation to that of other mice (Fig. 7*e*,*f*); however, the effects of excitatory neuron-specific *Rheb1* knockout were milder than those of lonafarnib treatment. This might be because Rheb1 activation is not suppressed in other cells, such as astrocytes, which

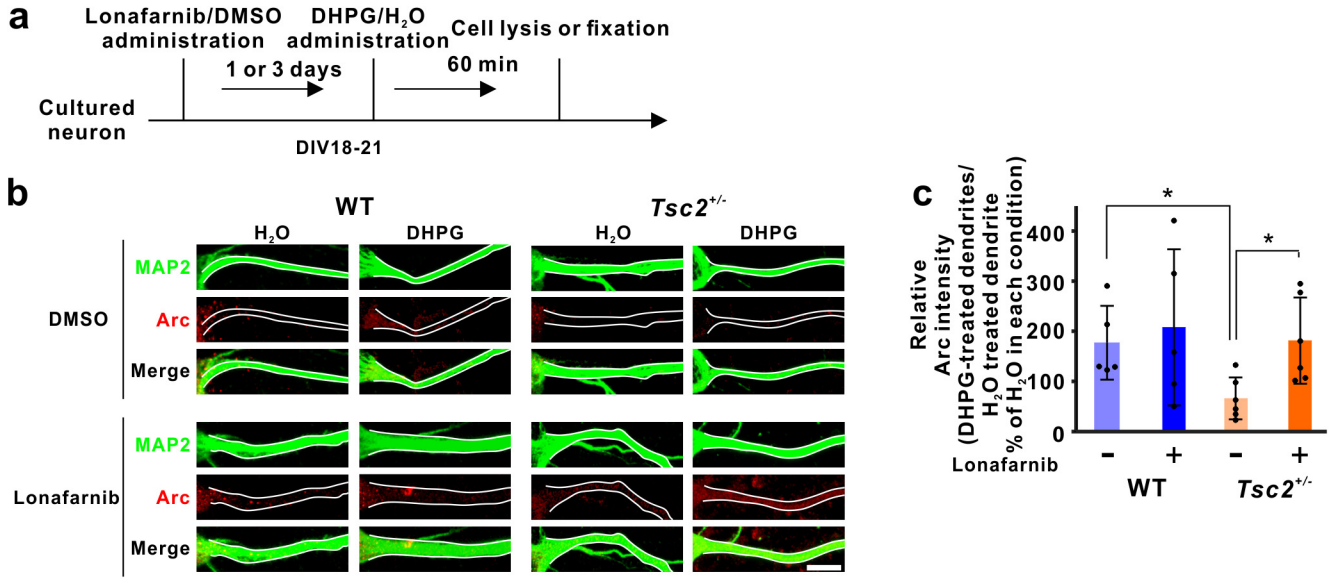

Figure 5. Arc protein synthesis in the dendrites of $Tsc2^{+/-}$ neurons was restored by lonafarnib treatment. ***a***, Schematic illustration of the experimental design to quantify the synthesis of the Arc protein. ***b***, Representative images of Arc staining in WT and $Tsc2^{+/-}$ hippocampal dendrites treated with DMSO (vehicle) or lonafarnib for 3 d and 60 min after DHPG or H_2O (vehicle) application. Scale bar, 5 μm. ***c***, Quantification of the dendritic Arc staining in ***b***. DHPG-treated Arc levels are divided by average H_2O-treated Arc levels [$n = 5$ (WT, DMSO, H_2O), $n = 5$ (WT, DMSO, DHPG), $n = 5$ (WT, lonafarnib, H_2O), $n = 5$ (WT, lonafarnib, DHPG), $n = 5$ ($Tsc2^{+/-}$, DMSO, H_2O), $n = 6$ ($Tsc2^{+/-}$, DMSO, DHPG), $n = 5$ ($Tsc2^{+/-}$, lonafarnib, H_2O), $n = 6$ ($Tsc2^{+/-}$, lonafarnib, DHPG), neurons, respectively; one-way ANOVA, *post hoc* Dunnett's test: $F_{(3,18)} = 1.739$, $^*p = 0.045$ (WT, DMSO vs $Tsc2^{+/-}$, DMSO); $^*p = 0.040$ ($Tsc2^{+/-}$, DMSO vs $Tsc2^{+/-}$, lonafarnib); two-way ANOVA, treatment × genotype interaction: $F_{(1,18)} = 1.071$, $p = 0.315$; genotype: $F_{(1,18)} = 2.826$, $p = 0.110$; treatment: $F_{(1,18)} = 3.189$, $p = 0.091$). $^*p < 0.05$.

could have contributed to the cognitive deficits. Furthermore, the Rheb1 hetero-knockout rescued the dendritic spine width in the *Tsc2*$^{+/-}$*;Cre* mice, without affecting dendritic spine density (Fig. 7*g–i*). We further investigated whether pharmacological inhibition has additive effect on the genetic deletion of Rheb1; in other words, whether genetic deletion of Rheb1 ameliorates cognitive deficits in *Tsc2*$^{+/-}$ mice as well as lonafarnib administration does. In histologic analysis, lonafarnib administration to *Tsc2*$^{+/-}$*;Rheb1-flox* mice did not increase spine width additionally *in vivo* (Fig. 8*a–c*). In behavioral analysis, lonafarnib administration to *Tsc2*$^{+/-}$*;Rheb1-flox* mice showed comparable results to those in vehicle-treated *Tsc2*$^{+/-}$*;Rheb1-flox* mice (Fig. 8*d*). Still, we cannot completely rule out the possibilities that lonafarnib affects other target proteins than Rheb1 to recover neuronal and behavioral disability; however, the main target protein of lonafarnib would be Rheb1 in *Tsc2*$^{+/-}$ mice because genetic Rheb1 deletion and lonafarnib treatment have sufficient effects on neuronal morphology and function recovery. Together, pharmacological and genetic inhibition of Rheb1 may be crucial for the restoration of synaptic and memory retrieval in *Tsc2*$^{+/-}$ mice.

Discussion

Here, we demonstrated that the activation of Rheb1, but not mTORC1, is involved in key aspects of synaptic and behavioral abnormalities in TSC model mice. Because pharmacological and genetic inhibition of Rheb1 restored synaptic and behavioral impairments in TSC mice, we investigated the detailed mechanism. First, lonafarnib treatment converted Rheb1 to its inactive, unfarnesylated form without affecting mTORC1 or MAP kinase signaling. Second, lonafarnib treatment restored plasticity-related Arc expression to control levels in both TSC neurons and mice. Finally, lonafarnib treatment corrected impaired memory engrams in the hippocampi of TSC mice. Collectively, activation of Rheb1 may disturb proper synapse and circuit formation, resulting in cognitive deficits in TSC. FTI treatment could ameliorate TAND-related intellectual disability through the restoration of synapses and memory engrams by Rheb1 inhibition. We show that the TSC–Rheb1 pathway impacts neuronal synapses and circuits, and provides insight into neurodevelopmental processes and potential treatment options for TAND symptoms.

FTIs have been developed to inhibit farnesylation of Ras proteins, since post-translational farnesylation is necessary for the membrane targeting of Ras proteins. Rheb1 also requires post-translational prenylation for its proper localization and activity (Buerger et al., 2006). Rheb1 has been shown to be localized to lysosomal membranes via its C-terminal farnesylation (Sancak et al., 2010). Tsc2 is released from Rheb1-localized lysosomal membranes in a growth factor-dependent or amino acid-dependent manner (Demetriades et al., 2016), leading to the activation of Rheb1. Thus, the farnesylation-mediated Rheb1 localization may be critical for its activation. This study showed that the inhibition of Rheb1 farnesylation restored synaptic abnormalities and cognitive deficits in *Tsc2*$^{+/-}$ neurons and mice, respectively, indicating that Rheb1 activation may be an underlying cause for the TAND symptoms of TSC patients.

FTIs can affect the activities of other signaling molecules; therefore, we cannot rule out the possibility that the beneficial effects of lonafarnib on cognition are because of the inhibition of other proteins. A variety of substrates other than Ras and Rheb1 are farnesylated, including lamin A, lamin B, RhoB, the centromere proteins CENP-E and CENP-F, and Rhes (Basso et al., 2005; Hernandez et al., 2019). Interestingly, lonafarnib was shown to ameliorate behavioral abnormalities in the tauopathy model via Rhes farnesylation (Hernandez et al., 2019). This contributing mechanism is lysosomal activation, which might be different from that of Rheb1 degradation (Sugiura et al., 2015). However, as lonafarnib-induced Rheb1 decreases are crucial for its actions (Fig. 2*a*), lysosomal involvement needs to be investigated. On the other hand, heterozygous knockout of the Rheb1 gene restored spine formation (Fig. 7*a–d*) and normal cognition

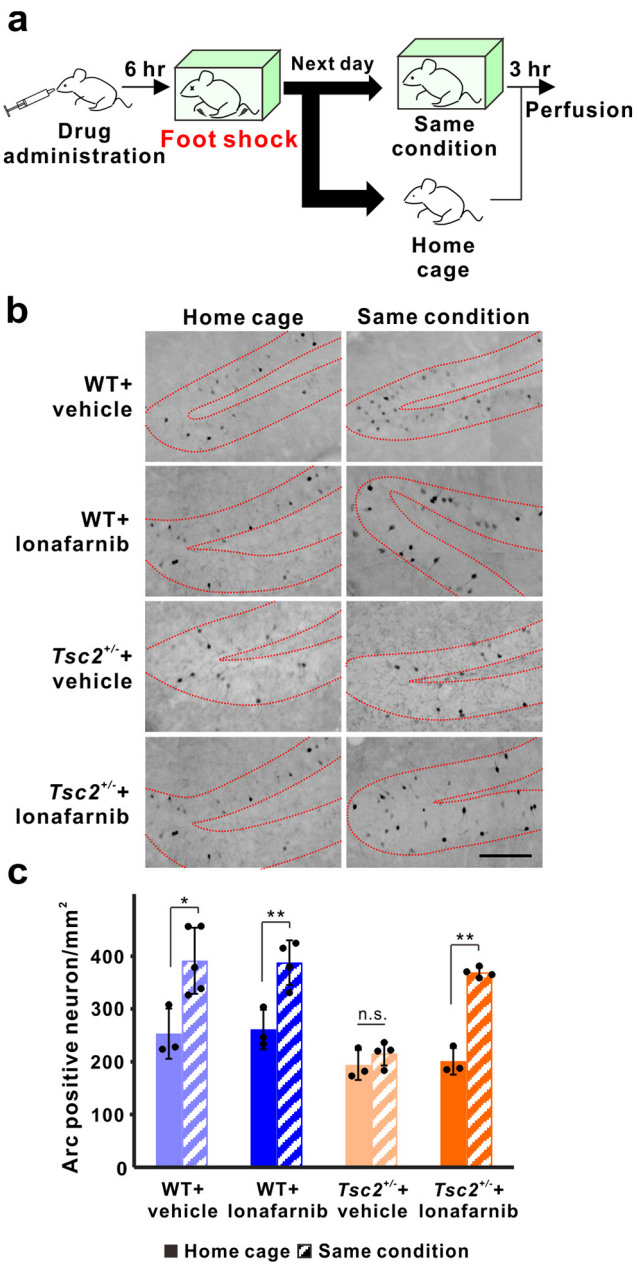

Figure 6. Lonafarnib-mediated recovery of memory encoding restored memory retrieval induced Arc expression in the hippocampi of *Tsc2*$^{+/-}$ mice. ***a***, Schematic illustration of the experimental design for the immunohistological analysis after the memory recall-inducing treatment. ***b***, Home cage-treated (basal) and same-condition-treated (memory-recall-induced) Arc expression in the DG of vehicle- or lonafarnib-administered WT and *Tsc2*$^{+/-}$ mice. Scale bar, 100 μm. ***c***, Quantification of Arc^{+} neurons in the DG. Vehicle-treated WT mice exhibited an increase in Arc^{+} neurons in the DG after memory recall, whereas vehicle-treated *Tsc2*$^{+/-}$ mice did not show a significant increase in Arc expression. Lonafarnib treatment restored Arc induction in the DG neurons of *Tsc2*$^{+/-}$ mice [hippocampi/animals for home cage and same condition, respectively; $n = 18/3$ and 30/5 (WT + vehicle), $n = 18/3$ and 32/4 (WT + lonafarnib), $n = 30/3$ and 17/4 (*Tsc2*$^{+/-}$ + vehicle), and $n = 18/3$ and 30/4 (*Tsc2*$^{+/-}$ + lonafarnib); two-tailed *t* test with Welch's correction: $t_{(5.407)} = 3.523$, $^{*}p = 0.015$ (WT + vehicle); $t_{(4.760)} = 4.175$, $^{**}p = 0.010$ (WT + lonafarnib); $t_{(3.781)} = 1.083$, $p = 0.343$ (*Tsc2*$^{+/-}$ + vehicle); $t_{(2.429)} = 710.964$, $^{**}p = 0.004$ (*Tsc2*$^{+/-}$ + lonafarnib); three-way ANOVA: genotype × treatment × induction interaction: $F_{(1,21)} = 6.928$, $p = 0.016$; genotype × treatment interaction: $F_{(1,21)} = 6.760$, $p = 0.017$; genotype × induction interaction: $F_{(1,21)} = 1.565$, $p = 0.225$; treatment × induction interaction: $F_{(1,21)} = 5.055$, $p = 0.035$; genotype: $F_{(1,21)} = 27.39$, $p < 0.001$; treatment: $F_{(1,21)} = 7.522$, $p = 0.012$; induction: $F_{(1,21)} = 57.32$, $p < 0.001$]. Data are averaged and presented by mouse type. Error bars indicate SD. $^{*}p < 0.05$, $^{**}p < 0.01$, n.s.: not significant.

(Fig. 7*e*,*f*) in *Tsc2*$^{+/-}$ neurons and mice, respectively. In addition, lonafarnib administration to *Tsc2*$^{+/-}$*;Rheb1-flox* mice had no or weak additive effect on spine formation and learning ability (Fig. 8); therefore, the activation of Rheb1 signaling in *Tsc2*$^{+/-}$ mice may be sufficient for the manifestation of cognitive deficits that these could be improved by FTI treatment. Furthermore, genetic deletion of farnesyltransferase has been shown to modify Alzheimer's disease neuropathology and to improve synaptic function and learning ability in animal models (Cheng et al., 2013; Jeong et al., 2021; Qu et al., 2021). Rheb1 was one of the substrate proteins that was enriched in the brains of farnesyltransferase knock-out mice (Qu et al., 2021).

Hyperactivity of the mTOR pathway in mice can lead to a myriad of phenotypes such as behavioral abnormalities. Several lines of evidence suggest that the mTOR pathway regulates long-term potentiation (LTP; Tang et al., 2002) and that increased mTOR signaling can change the induction of late-phase LTP, which most likely accounts for the learning and memory deficits in *Tsc2*$^{+/-}$ mice. Thus, mTOR inhibitors can improve the cognitive deficits associated with TSC. In fact, high-dose rapamycin (2–5 mg/kg) treatment reversed the contextual memory deficits in *Tsc2*$^{+/-}$ mice (Ehninger et al., 2008; Way et al., 2012). However, how upregulated mTORC1 signaling causes cognitive deficits in TSC mice remains unclear. Rapamycin did not restore spine synapse formation in *Tsc2*$^{+/-}$ neurons under our conditions (Fig. 1*e*–*h*). Other studies also showed that rapamycin treatment caused modest to robust increases in spine length in Tsc1 or Tsc2 knock-down neurons (Tavazoie et al., 2005; Meikle et al., 2008). Therefore, rapamycin could improve TSC-related cognitive deficits without restoring synaptic morphology. It might be possible that FTI restores memory deficits via partial inhibition of mTORC1 signaling, but its steady-state activity was not suppressed by lonafarnib treatment (Fig. 3*d*). Apart from cognitive function, rapamycin can prevent epilepsy in a mouse model of TSC (Zeng et al., 2008), whereas we failed to see that lonafarnib prevented PTZ-mediated seizure exacerbation (data not shown), indicating that FTI would exert its efficacy for ameliorating memory dysfunction in *Tsc2*$^{+/-}$ mice.

In contrast, lonafarnib restored the cognitive deficits in *Tsc2*$^{+/-}$ mice, probably through the correction of synaptic morphology and Arc expression. Impaired Arc induction might disturb mGluR5-dependent long-term plasticity in TSC neurons (Auerbach et al., 2011). Additionally, a reduction in the dendritic spines of memory engram cells was shown to be well correlated with memory impairments in a model of Alzheimer's disease (Roy et al., 2016). Therefore, impaired spine formation in *Tsc2*$^{+/-}$ mice might cause distorted engram connections in the DG, resulting in memory deficits.

We administered lonafarnib to the mice 6 h before footshock (learning) and tested their memory recall 24 h after footshock. As *Tsc2*$^{+/-}$ mice froze with the familiar context 30 h after lonafarnib administration, its effects appear to persist for at least 30 h. However, lonafarnib treatment after encoding did not increase discrimination ability in *Tsc2*$^{+/-}$ mice. Therefore, the administration of lonafarnib before learning is necessary for memory encoding. We speculate that pretreatment with lonafarnib can restore synaptic abnormalities by encoding (footshock plus context) and that its effects can persist until recall. The dendritic spine width at 24 h after administration was significantly greater in lonafarnib-treated mice than in vehicle-treated mice (Fig. 3*h*,*i*). Although the $T_{1/2}$ (biological half-life) of lonafarnib in the blood is approximately several hours, its effects in the brain might continue longer through the maintenance of dendritic

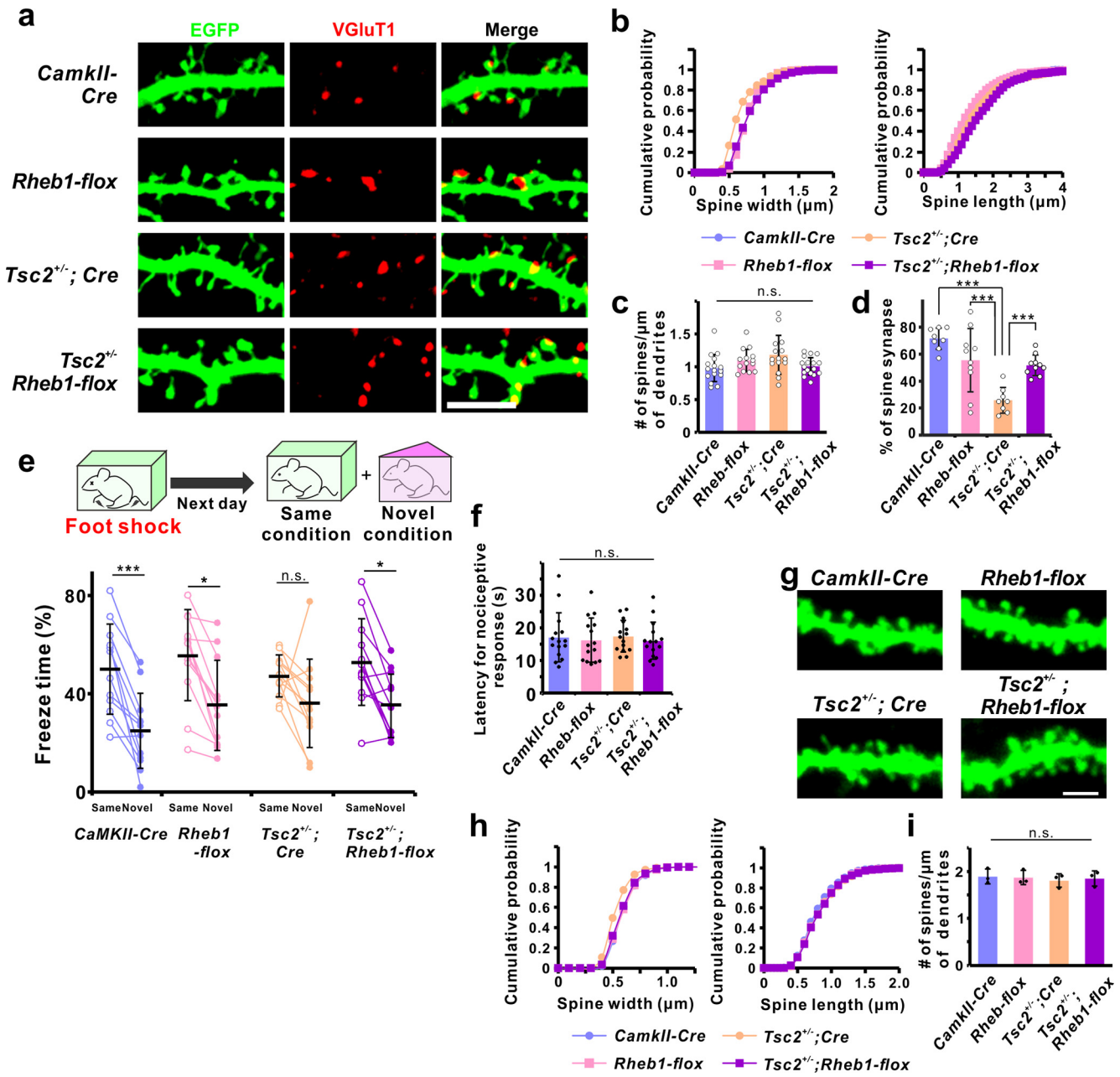

Figure 7. Heterozygous knockout of *Rheb1* mimicked the lonafarnib-mediated recovery of spine malformation in $Tsc2^{+/-}$ neurons and impaired fear memory in $Tsc2^{+/-}$ mice. ***a***, Confocal images of cultured hippocampal neurons from *CamkII-Cre*, *CamkII-Cre; Rheb1*$^{flox/+}$ (*Rheb1-flox*), $Tsc2^{+/-}$; *CamkII-Cre* ($Tsc2^{+/-}$; *Cre*), or $Tsc2^{+/-}$; *CamkII-Cre; Rheb1*$^{flox/+}$ ($Tsc2^{+/-}$; *Rheb1-flox*) mice. Immunodetection of VGluT1^{+} (red) presynaptic boutons on EGFP-expressing (green) neurons. Scale bar, 5 μm. ***b***, Cumulative probability distributions of the spine widths (left) and lengths (right) in ***a***. Note that heterozygous Rheb1 knockout increased the dendritic spine width ($D = 0.281$, $^{***}p < 0.001$) and decreased the dendritic spine length ($D = 0.095$, $^{*}p = 0.013$) in $Tsc2^{+/-}$ neurons [spines/neurons, respectively; $n = 564/16$ (*CamkII-Cre*), $n = 558/14$ (*Rheb1-flox*), $n = 552/15$ ($Tsc2^{+/-}$; *Cre*), and $n = 562/17$ ($Tsc2^{+/-}$; *Rheb1-flox*; Kolmogorov–Smirnov test)]. ***c***, Quantification of spine density in ***a*** [dendrites; $n = 16$ (*CamkII-Cre*), $n = 14$ (*Rheb1-flox*), $n = 15$ ($Tsc2^{+/-}$; *Cre*), and $n = 17$ ($Tsc2^{+/-}$; *Rheb1-flox*); one-way ANOVA, *post hoc* Tukey's test: $F_{(3,58)} = 0.548$, $p = 0.053$ (*CamkII-Cre* vs $Tsc2^{+/-}$; *Cre*)]. ***d***, Quantification of VGluT1^{+} spines in ***a***. Decrease of spine synapses with VGluT1 puncta in $Tsc2^{+/-}$; *Cre* neuron was restored in $Tsc2^{+/-}$; *Rheb1-flox* neurons [dendrites; $n = 8$ (*CamkII-Cre*), $n = 8$ (*Rheb1-flox*), $n = 10$ ($Tsc2^{+/-}$; *Cre*), and $n = 10$ ($Tsc2^{+/-}$; *Rheb1-flox*); one-way ANOVA: *post hoc* Tukey's test: $F_{(3,32)} = 14.061$; $^{***}p < 0.001$, $Tsc2^{+/-}$; *Cre* vs *CamkII-Cre*; $^{***}p < 0.001$, $Tsc2^{+/-}$; *Cre* vs *Rheb1-flox*; $^{***}p = 0.003$, $Tsc2^{+/-}$; *Cre* vs $Tsc2^{+/-}$; *Rheb1-flox*]. ***e***, Heterozygous Rheb1 knockout rescued the memory deficits of $Tsc2^{+/-}$ mice. *CamkII-Cre* mice showed intact memory by freezing more in the familiar context than in the novel context ($n = 12$ animals; $t_{(21.315)} = 3.648$, $^{***}p = 0.002$), whereas $Tsc2^{+/-}$; *Cre* mice showed impaired contextual discrimination ($n = 12$ animals; $t_{(15.688)} = 1.908$, $p = 0.075$). Heterozygous Rheb1 knockout rescued the deficit in contextual discrimination ($n = 12$ animals; $t_{(20.108)} = 2.797$, $^{*}p = 0.011$), and *Rheb1-flox* mice exhibited normal memory ($n = 12$ animals; $t_{(21.998)} = 2.678$, $^{*}p = 0.014$), two-tailed *t* test with Welch's correction. Two-way ANOVA: genotype × apparatus interaction: $F_{(3,88)} = 0.789$, $p = 0.503$; genotype: $F_{(3,88)} = 1.143$, $p = 0.336$; apparatus: $F_{(1,88)} = 30.88$, $p < 0.001$). ***f***, The hot plate test indicated no significant difference in the time for a nociceptive response among *CamkII-Cre*, *Rheb1-flox*, $Tsc2^{+/-}$; *Cre*, and $Tsc2^{+/-}$; *Rheb1-flox* mice (one-way ANOVA; $n = 15$ animals; $F_{(3,56)} = 0.169$, $p = 0.917$). ***g***, Representative DiI-labeled dendrites from the hippocampal CA1 neurons of *CamkII-Cre*, *Rheb1-flox*, $Tsc2^{+/-}$; *Cre*, or $Tsc2^{+/-}$; *Rheb1-flox* mice. Scale bar, 2 μm. ***h***, Cumulative probability plots of the spine width (left) and spine length (right) in ***g***. $Tsc2^{+/-}$; *Cre* neurons showed a decreased spine width ($D = 0.227$; $^{***}p < 0.001$, $Tsc2^{+/-}$; *Cre* vs *CamkII-Cre*), and heterozygous Rheb1 knockout rescued the aberrant spine width [$D = 0.179$; $^{***}p < 0.001$, $Tsc2^{+/-}$; *Cre* vs $Tsc2^{+/-}$; spines/neurons/animals, respectively; *Rheb1-flox*; $n = 1035/26/3$ (*CamkII-Cre*), $n = 1027/25/3$ (*Rheb1-flox*), $n = 1016/29/3$ ($Tsc2^{+/-}$; *Cre*), and $n = 1029/30/3$ ($Tsc2^{+/-}$; *Rheb1-flox*); Kolmogorov–Smirnov test)]. ***i***, Quantification of spine density in ***g*** [neurons/animals, respectively; $n = 26/3$ (*CamkII-Cre*), $n = 25/3$ (*Rheb1-flox*), $n = 29/3$ ($Tsc2^{+/-}$; *Cre*), and $n = 30/3$ ($Tsc2^{+/-}$; *Rheb1-flox*); one-way ANOVA, *post hoc* Tukey's test: $F_{(3,\ 8)} = 0.175$ $p = 0.910$]. Data are averaged and presented by mice. Error bars indicate SD. $^{*}p < 0.05$, $^{***}p < 0.005$, n.s.: not significant. D: the largest absolute difference between the two distribution functions across all values.

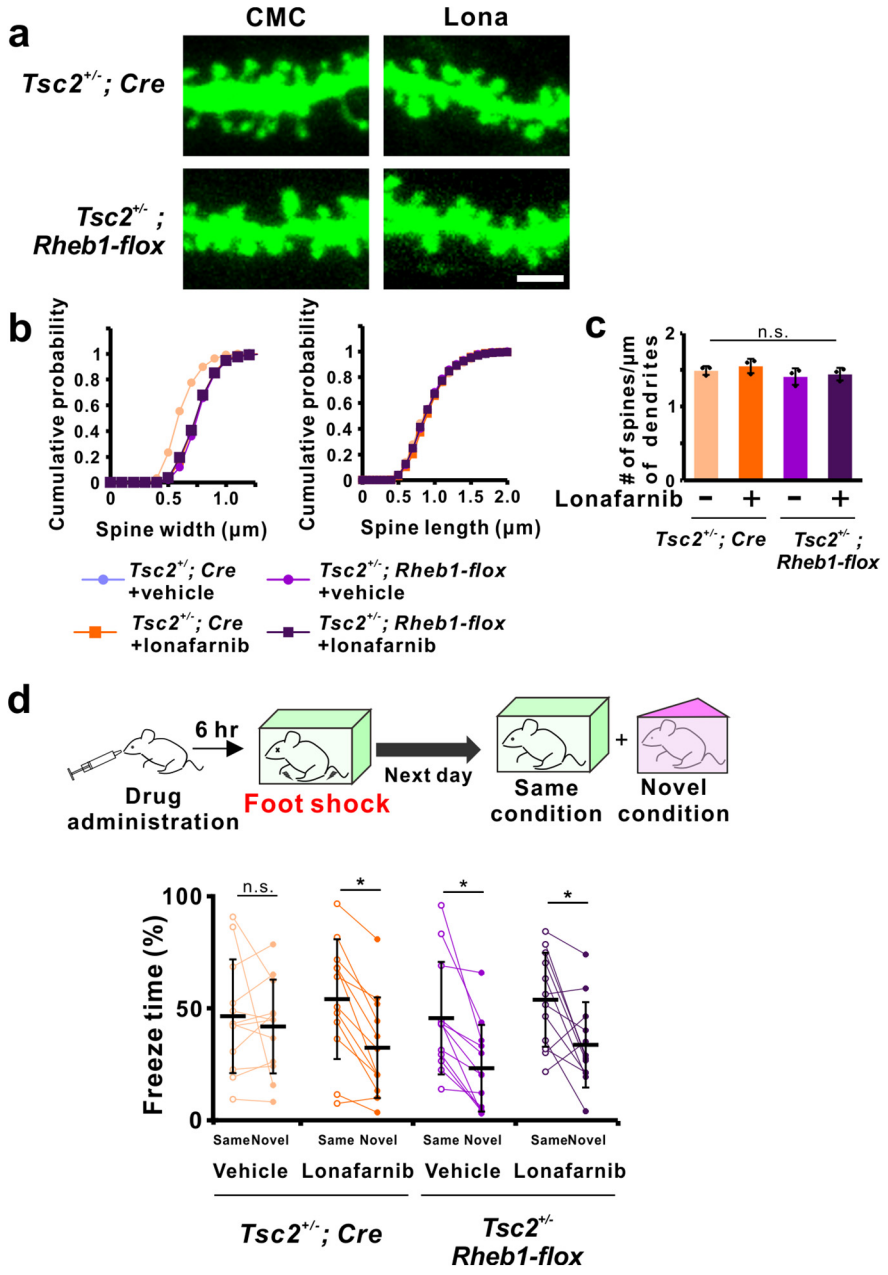

Figure 8. Lonafarnib administration had no or weak effect on heterozygous knockout of *Rheb1* in the recovery of spine malformation in $Tsc2^{+/-}$ neurons and impaired fear memory in $Tsc2^{+/-}$ mice. ***a***, Representative DiI-labeled dendrites from the hippocampal CA1 neurons of vehicle- or lonafarnib-administered $Tsc2^{+/-}$; *CamkII-Cre* ($Tsc2^{+/-}$; *Cre*) and $Tsc2^{+/-}$; *CamkII-Cre*; $Rheb1^{flox/+}$ ($Tsc2^{+/-}$; *Rheb1-flox*) mice. Scale bar, 2 μm. ***b***, Cumulative probability plots of the spine width (left) and spine length (right) in ***a***. $Tsc2^{+/-}$; *Rheb1-flox* + lonafarnib neurons showed a comparable spine width to $Tsc2^{+/-}$; *Cre* + lonafarnib neurons and $Tsc2^{+/-}$; *Rheb1-flox* + vehicle neurons [D = 0.033, $p = 0.638$ ($Tsc2^{+/-}$; *Rheb1-flox* + lonafarnib vs $Tsc2^{+/-}$; *Cre* + lonafarnib); D = 0.009, ***$p < 0.001$ ($Tsc2^{+/-}$; *Rheb1-flox* + lonafarnib vs $Tsc2^{+/-}$; *Rheb1-flox* + vehicle; $Tsc2^{+/-}$; *Rheb1-flox* + vehicle showed wider average; spines/neurons/animals, respectively: $n = 1038/26/3$ ($Tsc2^{+/-}$; *Cre* + vehicle), $n = 1027/26/3$ ($Tsc2^{+/-}$; *Cre* + lonafarnib), $n = 1008/29/3$ ($Tsc2^{+/-}$; *Rheb1-flox* + vehicle), and $n = 1023/26/3$ ($Tsc2^{+/-}$; *Rheb1-flox* + lonafarnib); Kolmogorov–Smirnov test]. ***c***, Quantification of spine density in ***a*** [neurons/animals, respectively; $n = 26/3$ ($Tsc2^{+/-}$; *Cre* + vehicle), $n = 26/3$ ($Tsc2^{+/-}$; *Cre* + lonafarnib), $n = 29/3$ ($Tsc2^{+/-}$; *Rheb1-flox* + vehicle), and $n = 26/3$ ($Tsc2^{+/-}$; *Rheb1-flox* + lonafarnib); one-way ANOVA: $F_{(3,8)} = 1.440$, $p = 0.302$; two-way ANOVA, treatment × genotype interaction: $F_{(1,8)} = 0.071$, $p = 0.797$; genotype: $F_{(1,8)} = 3.418$, $p = 0.102$; treatment: $F_{(1,8)} = 0.830$, $p = 0.389$; data are averaged and presented by mouse type]. ***d***, Schematic illustration of the experimental design for the contextual learning task. $Tsc2^{+/-}$; *Rheb1-flox* + lonafarnib mice showed a comparable phenotype of learning ability to $Tsc2^{+/-}$; *Cre* + lonafarnib mice and $Tsc2^{+/-}$; *Rheb1-flox* + vehicle mice ($n = 12$ animals; two-tailed *t* test with Welch's correction: $t_{(21.225)} = 0.483$, $p = 0.638$ ($Tsc2^{+/-}$; *Cre* + vehicle); $t_{(21.359)} = 2.149$, *$p = 0.043$ ($Tsc2^{+/-}$; *Cre* + lonafarnib); $t_{(20.661)} = 2.444$, *$p = 0.024$ ($Tsc2^{+/-}$; *Rheb1-flox* + vehicle); $t_{(21.799)} = 2.462$, *$p = 0.022$ ($Tsc2^{+/-}$; *Rheb1-flox* + lonafarnib); three-way ANOVA: genotype × treatment × apparatus interaction: $F_{(1,88)} = 1.088$, $p = 0.300$; genotype × treatment interaction: $F_{(1,88)} = 1.235$, $p = 0.269$; genotype × apparatus interaction: $F_{(1,88)} = 0.770$, $p = 0.383$; treatment × apparatus interaction: $F_{(1,88)} = 0.644$, $p = 0.424$; genotype: $F_{(1,88)} = 1.000$, $p = 0.320$; treatment: $F_{(1,88)} = 0.829$, $p = 0.365$; apparatus: $F_{(1,88)} = 13.80$, $p < 0.001$; multiple comparison after three-way ANOVA: *post hoc* Sidak's test: $p = 0.998$ (same: $Tsc2^{+/-}$; *Cre* + vehicle vs $Tsc2^{+/-}$; *Cre* + lonafarnib); $p = 0.988$ (novel: $Tsc2^{+/-}$; *Cre* + vehicle vs $Tsc2^{+/-}$; *Cre* + lonafarnib); $p = 0.997$ (same: $Tsc2^{+/-}$; *Rheb1-flox* + vehicle vs $Tsc2^{+/-}$; *Rheb1-flox* + lonafarnib); $p = 0.735$ (novel: $Tsc2^{+/-}$; *Rheb1-flox* + vehicle vs $Tsc2^{+/-}$; *Rheb1-flox* + lonafarnib)]. Error bars indicate SD. *$p < 0.05$, n.s.: not significant. D: the largest absolute difference between the two distribution functions across all values.

spine morphology. We could not find significant increases of unfarnesylated Rheb1 and decreases of total Rheb1 in the lonafarnib-administered mouse brain by Western blot, but lonafarnib treatment recovered abnormal neuronal morphology and memory-encoding dysfunction, indicating lonafarnib could penetrate the blood–brain barrier. This might suggest that Rheb1 in the neurons is easier to be unfarnesylated by lonafarnib than that in the glial cells, and unfarnesylated Rheb1 is rather sensitive to proteasomal degradation during biochemical sampling *in vivo*.

Clinical investigations of TSC patients have been performed with the rapamycin analog everolimus. SEGA regression was demonstrated in a double-blind, placebo-controlled phase III trial. In another study, the seizure frequency was lower in TSC patients with refractory seizures who were treated with everolimus than in those treated with placebo as a control (Krueger et al., 2013). However, everolimus treatment has not yet improved neurocognitive symptoms so far (Overwater et al., 2019). This failure might be because everolimus was not administered at a critical window of efficacy (Ehninger et al., 2009; Way et al., 2012). In addition, some adverse effects of everolimus, such as stomatitis, pharyngitis, pneumonia, vomiting, and decreased appetite, have been reported (Franz et al., 2013; French et al., 2016). On the other hand, lonafarnib has been used to treat progeria and hepatitis D in clinical trials, and both studies provided evidence for the efficacy and relatively low toxicity of lonafarnib (Koh et al., 2015; Gordon et al., 2018). Because neuronal Rheb1 expression is upregulated by epileptic seizures (Yamagata et al., 1994) and high expression of constitutively active Rheb1 in the brain displayed spontaneous, recurrent seizures (Hsieh et al., 2016; Nguyen et al., 2019),

epilepsy-related cognitive problems could also be a therapeutic target for lonafarnib. Our observations may corroborate how Rheb1 protein can inform biological mechanisms underlying common traits in the neurodevelopmental disorders. We speculate that targeted administration of lonafarnib, perhaps during critical postnatal neurodevelopmental windows, might be of significant benefit to patients. Its safety profile may promote this drug to a promising candidate for treatment of intractable cognitive deficits in TSC patients.

References

Auerbach BD, Osterweil EK, Bear MF (2011) Mutations causing syndromic autism define an axis of synaptic pathophysiology. Nature 480:63–68.

Basso AD, Mirza A, Liu G, Long BJ, Bishop WR, Kirschmeier P (2005) The farnesyl transferase inhibitor (FTI) SCH66336 (lonafarnib) inhibits Rheb farnesylation and mTOR signaling. Role in FTI enhancement of taxane and tamoxifen anti-tumor activity. J Biol Chem 280:31101–31108.

Bateup HS, Takasaki KT, Saulnier JL, Denefrio CL, Sabatini BL (2011) Loss of Tsc1 *in vivo* impairs hippocampal mGluR-LTD and increases excitatory synaptic function. J Neurosci 31:8862–8869.

Buerger C, DeVries B, Stambolic V (2006) Localization of Rheb to the endomembrane is critical for its signaling function. Biochem Biophys Res Commun 344:869–880.

Casey PJ, Seabra MC (1996) Protein prenyltransferases. J Biol Chem 271:5289–5292.

Cheng S, Cao D, Hottman DA, Yuan L, Bergo MO, Li L (2013) Farnesyltransferase haplodeficiency reduces neuropathology and rescues cognitive function in a mouse model of Alzheimer disease. J Biol Chem 288:35952–35960.

Chowdhury S, Shepherd JD, Okuno H, Lyford G, Petralia RS, Plath N, Kuhl D, Huganir RL, Worley PF (2006) Arc/Arg3.1 interacts with the endocytic machinery to regulate AMPA receptor trafficking. Neuron 52:445–459.

Clark GJ, Kinch MS, Rogers-Graham K, Sebti SM, Hamilton AD, Der CJ (1997) The Ras-related protein Rheb is farnesylated and antagonizes Ras signaling and transformation. J Biol Chem 272:10608–10615.

Curatolo P, Bombardieri R, Jozwiak S (2008) Tuberous sclerosis. Lancet 372:657–668.

Curatolo P, Moavero R, de Vries PJ (2015) Neurological and neuropsychiatric aspects of tuberous sclerosis complex. Lancet Neurol 14:733–745.

Demetriades C, Plescher M, Teleman AA (2016) Lysosomal recruitment of TSC2 is a universal response to cellular stress. Nat Commun 7:10662.

Ehninger D, Han S, Shilyansky C, Zhou Y, Li W, Kwiatkowski DJ, Ramesh V, Silva AJ (2008) Reversal of learning deficits in a $Tsc2^{+/-}$ mouse model of tuberous sclerosis. Nat Med 14:843–848.

Ehninger D, de Vries PJ, Silva AJ (2009) From mTOR to cognition: molecular and cellular mechanisms of cognitive impairments in tuberous sclerosis. J Intellect Disabil Res 53:838–851.

Franz DN, Belousova E, Sparagana S, Bebin EM, Frost M, Kuperman R, Witt O, Kohrman MH, Flamini JR, Wu JY, Curatolo P, de Vries PJ, Whittemore VH, Thiele EA, Ford JP, Shah G, Cauwel H, Lebwohl D, Sahmoud T, Jozwiak S (2013) Efficacy and safety of everolimus for subependymal giant cell astrocytomas associated with tuberous sclerosis complex (EXIST-1): a multicentre, randomised, placebo-controlled phase 3 trial. Lancet 381:125–132.

French JA, Lawson JA, Yapici Z, Ikeda H, Polster T, Nabbout R, Curatolo P, de Vries PJ, Dlugos DJ, Berkowitz N, Voi M, Peyrard S, Pelov D, Franz DN (2016) Adjunctive everolimus therapy for treatment-resistant focal-onset seizures associated with tuberous sclerosis (EXIST-3): a phase 3, randomised, double-blind, placebo-controlled study. Lancet 388:2153–2163.

Gordon LB, Shappell H, Massaro J, D'Agostino RB Sr, Brazier J, Campbell SE, Kleinman ME, Kieran MW (2018) Association of lonafarnib treatment vs no treatment with mortality rate in patients with Hutchinson-Gilford progeria syndrome. JAMA 319:1687–1695.

Guzowski JF, Setlow B, Wagner EK, McGaugh JL (2001) Experience-dependent gene expression in the rat hippocampus after spatial learning: a comparison of the immediate-early genes *Arc*, c-*fos*, and *zif268*. J Neurosci 21:5089–5098.

Hernandez I, Luna G, Rauch JN, Reis SA, Giroux M, Karch CM, Boctor D, Sibih YE, Storm NJ, Diaz A, Kaushik S, Zekanowski C, Kang AA, Hinman CR, Cerovac V, Guzman E, Zhou H, Haggarty SJ, Goate AM, Fisher SK, et al (2019) A farnesyltransferase inhibitor activates lysosomes and reduces tau pathology in mice with tauopathy. Sci Transl Med 11: eaat3005.

Hsieh LS, Wen JH, Claycomb K, Huang Y, Harrsch FA, Naegele JR, Hyder F, Buchanan GF, Bordey A (2016) Convulsive seizures from experimental focal cortical dysplasia occur independently of cell misplacement. Nat Commun 7:11753.

Iffland PH 2nd, Carson V, Bordey A, Crino PB (2019) GATORopathies: the role of amino acid regulatory gene mutations in epilepsy and cortical malformations. Epilepsia 60:2163–2173.

Inoki K, Zhu TQ, Guan KL (2003) TSC2 mediates cellular energy response to control cell growth and survival. Cell 115:577–590.

Jeong A, Cheng S, Zhong R, Bennett DA, Bergö MO, Li L (2021) Protein farnesylation is upregulated in Alzheimer's human brains and neuron-specific suppression of farnesyltransferase mitigates pathogenic processes in Alzheimer's model mice. Acta Neuropathol Commun 9:129.

Kobayashi T, Minowa O, Kuno J, Mitani H, Hino O, Noda T (1999) Renal carcinogenesis, hepatic hemangiomatosis, and embryonic lethality caused by a germ-line Tsc2 mutation in mice. Cancer Res 59:1206–1211.

Koh C, Canini L, Dahari H, Zhao X, Uprichard SL, Haynes-Williams V, Winters MA, Subramanya G, Cooper SL, Pinto P, Wolff EF, Bishop R, Ai Thanda Han M, Cotler SJ, Kleiner DE, Keskin O, Idilman R, Yurdaydin C, Glenn JS, et al (2015) Oral prenylation inhibition with lonafarnib in chronic hepatitis D infection: a proof-of-concept randomised, double-blind, placebo-controlled phase 2A trial. Lancet Infect Dis 15:1167–1174.

Krueger DA, Wilfong AA, Holland-Bouley K, Anderson AE, Agricola K, Tudor C, Mays M, Lopez CM, Kim MO, Franz DN (2013) Everolimus treatment of refractory epilepsy in tuberous sclerosis complex. Ann Neurol 74:679–687.

Lipton JO, Sahin M (2014) The neurology of mTOR. Neuron 84:275–291.

Mahoney SJ, Narayan S, Molz L, Berstler LA, Kang SA, Vlasuk GP, Saiah E (2018) A small molecule inhibitor of Rheb selectively targets mTORC1 signaling. Nat Commun 9:548.

Meikle L, Pollizzi K, Egnor A, Kramvis I, Lane H, Sahin M, Kwiatkowski DJ (2008) Response of a neuronal model of tuberous sclerosis to mammalian target of rapamycin (mTOR) inhibitors: effects on mTORC1 and Akt signaling lead to improved survival and function. J Neurosci 28:5422–5432.

Nguyen LH, Mahadeo T, Bordey A (2019) mTOR hyperactivity levels influence the severity of epilepsy and associated neuropathology in an experimental model of tuberous sclerosis complex and focal cortical dysplasia. J Neurosci 39:2762–2773.

Osterweil EK, Chuang SC, Chubykin AA, Sidorov M, Bianchi R, Wong RK, Bear MF (2013) Lovastatin corrects excess protein synthesis and prevents epileptogenesis in a mouse model of fragile X syndrome. Neuron 77:243–250.

Overwater IE, Rietman AB, Mous SE, Bindels-de Heus K, Rizopoulos D, Ten Hoopen LW, van der Vaart T, Jansen FE, Elgersma Y, Moll HA, de Wit MY (2019) A randomized controlled trial with everolimus for IQ and autism in tuberous sclerosis complex. Neurology 93:e200–e209.

Penzes P, Cahill ME, Jones KA, VanLeeuwen JE, Woolfrey KM (2011) Dendritic spine pathology in neuropsychiatric disorders. Nat Neurosci 14:285–293.

Qu W, Suazo KF, Liu W, Cheng S, Jeong A, Hottman D, Yuan LL, Distefano MD, Li L (2021) Neuronal protein farnesylation regulates hippocampal synaptic plasticity and cognitive function. Mol Neurobiol 58:1128–1144.

Reijnders MRF, Kousi M, van Woerden GM, Klein M, Bralten J, Mancini GMS, van Essen T, Proietti-Onori M, Smeets EEJ, van Gastel M, Stegmann APA, Stevens SJC, Lelieveld SH, Gilissen C, Pfundt R, Tan PL, Kleefstra T, Franke B, Elgersma Y, Katsanis N, et al (2017) Variation in a range of mTOR-related genes associates with intracranial volume and intellectual disability. Nat Commun 8:1052.

Roy DS, Arons A, Mitchell TI, Pignatelli M, Ryan TJ, Tonegawa S (2016) Memory retrieval by activating engram cells in mouse models of early Alzheimer's disease. Nature 531:508–512.

Sancak Y, Bar-Peled L, Zoncu R, Markhard AL, Nada S, Sabatini DM (2010) Ragulator-Rag complex targets mTORC1 to the lysosomal surface and is necessary for its activation by amino acids. Cell 141:290–303.

Sugiura H, Yasuda S, Katsurabayashi S, Kawano H, Endo K, Takasaki K, Iwasaki K, Ichikawa M, Kobayashi T, Hino O, Yamagata K (2015) Rheb

activation disrupts spine synapse formation through accumulation of syntenin in tuberous sclerosis complex. Nat Commun 6:6842.

Tang SJ, Reis G, Kang H, Gingras AC, Sonenberg N, Schuman EM (2002) A rapamycin-sensitive signaling pathway contributes to long-term synaptic plasticity in the hippocampus. Proc Natl Acad Sci U S A 99:467–472.

Tavazoie SF, Alvarez VA, Ridenour DA, Kwiatkowski DJ, Sabatini BL (2005) Regulation of neuronal morphology and function by the tumor suppressors Tsc1 and Tsc2. Nat Neurosci 8:1727–1734.

Vazdarjanova A, Guzowski JF (2004) Differences in hippocampal neuronal population responses to modifications of an environmental context: evidence for distinct, yet complementary, functions of CA3 and CA1 ensembles. J Neurosci 24:6489–6496.

Wang X, Fonseca BD, Tang H, Liu R, Elia A, Clemens MJ, Bommer U-A, Proud CG (2008) Re-evaluating the roles of proposed modulators of mammalian target of rapamycin complex 1 (mTORC1) signaling. J Biol Chem 283:30482–30492.

Waung MW, Pfeiffer BE, Nosyreva ED, Ronesi JA, Huber KM (2008) Rapid translation of Arc/Arg3.1 selectively mediates mGluR-dependent LTD through persistent increases in AMPAR endocytosis rate. Neuron 59:84–97.

Way SW, Rozas NS, Wu HC, McKenna J 3rd, Reith RM, Hashmi SS, Dash PK, Gambello MJ (2012) The differential effects of prenatal and/or postnatal rapamycin on neurodevelopmental defects and cognition in a neuroglial mouse model of tuberous sclerosis complex. Hum Mol Genet 21:3226–3236.

Whyte DB, Kirschmeier P, Hockenberry TN, Nunez-Oliva I, James L, Catino JJ, Bishop WR, Pai JK (1997) K- and N-Ras are geranylgeranylated in cells treated with farnesyl protein transferase inhibitors. J Biol Chem 272:14459–14464.

Yamagata K, Sanders LK, Kaufmann WE, Yee W, Barnes CA, Nathans D, Worley PF (1994) rheb, a growth factor- and synaptic activity-regulated gene, encodes a novel Ras-related protein. J Biol Chem 269:16333–16339.

Yasuda S, Sugiura H, Katsurabayashi S, Shimada T, Tanaka H, Takasaki K, Iwasaki K, Kobayashi T, Hino O, Yamagata K (2014) Activation of Rheb, but not of mTORC1, impairs spine synapse morphogenesis in tuberous sclerosis complex. Sci Rep 4:5155.

Zeng L-H, Xu L, Gutmann DH, Wong M (2008) Rapamycin prevents epilepsy in a mouse model of tuberous sclerosis complex. Ann Neurol 63:444–453.

Zou J, Zhou L, Du X-X, Ji Y, Xu J, Tian J, Jiang W, Zou Y, Yu S, Gan L, Luo M, Yang Q, Cui Y, Yang W, Xia X, Chen M, Zhao X, Shen Y, Chen PY, Worley PF, et al (2011) Rheb1 is required for mTORC1 and myelination in postnatal brain development. Dev Cell 20:97–108.